Quantification of methane emissions in Hamburg using a network of FTIR spectrometers and an inverse modeling approach

Andreas Forstmaier[1], Jia Chen[1], Florian Dietrich[1], Juan Bettinelli[1], Hossein Maazallahi[2,5], Carsten Schneider[2,4], Dominik Winkler[1], Xinxu Zhao[1], Taylor Jones[6], Carina van der Veen[2], Norman Wildmann[3], Moritz Makowski[1], Aydin Uzun[1], Friedrich Klappenbach[1], Hugo Denier van der Gon[5], Stefan Schwietzke[7], and Thomas Röckmann[2]

[1]Environmental Sensing and Modeling, Technical University of Munich (TUM), Munich, Germany
[2]Institute for Marine and Atmospheric research Utrecht (IMAU), Utrecht University (UU), Utrecht, the Netherlands
[3]Deutsches Zentrum für Luft- und Raumfahrt (DLR), Institut für Physik der Atmosphäre, Oberpfaffenhofen, Germany
[4]Institut für Umweltphysik, University of Heidelberg, Heidelberg, Germany
[5]Netherlands Organisation for Applied Scientific Research (TNO), Utrecht, the Netherlands
[6]Earth and Environment, Boston University, Boston, United States
[7]Environmental Defense Fund, Berlin, Germany

Correspondence: Jia Chen (jia.chen@tum.de), Andreas Forstmaier (andreas.forstmaier@tum.de) and Florian Dietrich (flo.dietrich@tum.de)

Abstract. Methane (CH_4) is a potent greenhouse gas and anthropogenic CH_4 emissions contribute significantly to global warming. In this study, the CH_4 emissions of the second most populated city in Germany, Hamburg, were quantified with measurements from four solar-viewing Fourier Transform Infrared Spectrometers (FTIR), mobile in-situ measurements and an inversion framework. For source type attribution an Isotope Ratio Mass Spectrometer was deployed in the city. The urban district hosts an extensive industrial and port area in the south, as well as a large conglomerate of residential areas north of the Elbe river. For emission modeling the TNO GHGco inventory was used as a basis. In order to improve the inventory, two approaches were followed: Firstly the addition of a large natural CH_4 source, the Elbe river, which was previously not in the inventory. Secondly mobile measurements were carried out to update the spatial distribution of emissions in the TNO GHGco gridded inventory and derive two updated versions of the inventory. The addition of the river emissions improved model performance, while the correction of the spatial distribution with mobile measurements did not have a significant effect on the total emission estimates for the campaign period. A comparison of the updated inventories with emission estimates from a Gaussian Plume Model (GPM) showed that the updated versions of the inventory in several cases match the GPM emissions estimates well, revealing the potential of mobile measurements to update the spatial distribution of emission inventories. The mobile measurement survey also revealed a large, so far unknown point source in a refinery of thermogenic origin with a magnitude of 7.9 $\pm$5.3 kg h^{-1}. The isotopic measurements show strong indications that there is a large biogenic CH_4 source in Hamburg which produced repeated enhancements of over 1 ppm that correlate with the rising tide of the river estuary. The CH_4 emissions (anthropogenic and natural) of the city of Hamburg were quantified as 1600 $\pm$920 kg h^{-1} of which 900 $\pm$510 kg h^{-1} are of anthropogenic origin. This study reveals that mobile measurements at street-level may miss the majority of total methane emissions, potentially due to sources within buildings including stoves and boilers operating on natural gas. Similarly, the CH_4

20 enhancements recorded during the mobile survey from large area sources, like for instance the Alster lake, were too small to generate GPM emission estimates with confidence, but could nevertheless influence the total column emission estimates.

1 Introduction

Climate change has a profound impact on living conditions and human societies globally. To a large extent, it is driven by strong anthropogenic greenhouse gas (GHG) emissions. Methane (CH_4) is the second-most prevalent GHG emitted by human

25 activities (Allen et al., 2013). Over a 20-year horizon, the Intergovernmental Panel on Climate Change (IPCC) estimated the global warming potential (GWP) of CH_4 to be 84 times larger than that of Carbon Dioxide (CO_2) (IPCC et al., 2014). Methane has a relatively short atmospheric lifetime of about 9.1 ± 0.9 years (Prather et al., 2012), which makes it an attractive target to diminish the warming rates in the short- and medium-term.

In urban areas, there are various types of anthropogenic and natural CH_4 sources. Anthropogenic sources comprise fossil

30 fuel related emissions, such as fugitive emissions from gas pipelines (Schwietzke et al., 2014; McKain et al., 2015), or road transport and combustion of CH_4 (Defratyka et al., 2021) as well as biogenic emissions from sewage systems (Fernandez et al., 2022) and waste water treatment (Maazallahi et al., 2020). Furthermore, wetlands and bodies of water are common natural CH_4 emitters. For instance, in Hamburg, Matousu et al. (2017) showed that the river Elbe releases CH_4, and wetlands surrounding the Elbe produce CH_4, too (Ragnhild Hummel, 2021).

35 Given the range of possible sources, there are various methodologies used to quantify CH_4 emissions from gas pipelines, power plants, refineries and natural sources. To detect leak indications (LIs) for pipelines, frequently mobile measurements are applied, as shown by Maazallahi et al. (2020), who identified 145 LIs (i.e., CH_4 enhancements of more than 10 % above background levels) in Hamburg and 81 LIs in Utrecht while measuring CH_4 mole fractions at the street level. Data from such mobile surveys can then be further analyzed to quantify emissions from concentration measurements (Weller et al., 2019).

40 Similiarly, Phillips et al. (2013) identified 3356 LIs with concentrations exceeding up to 15 times the global background level through mapping CH_4 LIs across all urban roads in the city of Boston. Moreover, they associated the LIs with natural gas after analyzing the isotopic signatures. Weller et al. (2018) evaluated the ability of a mobile survey methodology (von Fischer et al., 2017) to detect natural gas leaks and quantify their emissions. Yacovitch et al. (2015) measured CH_4 and ethane (C_2H_6) concentrations in a mobile laboratory downwind of natural gas facilities in the Barnett Shale region. To quantify emissions

45 from a natural-gas-based power plant in Munich, Toja-Silva et al. (2017) employed differential column measurements (Chen et al., 2016), together with a computational fluid dynamics model. A study by Chen et al. (2020) revealed CH_4 emissions at a large folk festival, the Munich Oktoberfest in 2018 using mobile in-situ measurements.

Isolated CH_4 sources can be quantified best individually and this can gradually lead to a better understanding of the mix of sources in a certain area. At a city scale, the mix of sources can however become quite complex. Also above ground-

50 level sources, which cannot be picked up very well using ground-based mobile surveys, can play a role in the mixture of total emissions. Quantifying emissions of larger areas, thus entails the use of modeling frameworks, which incorporate wind information and mixing between a multitude of individual sources.

To determine natural gas emission rates for the Boston urban area, McKain et al. (2015) and Sargent et al. (2021) incorporated a high-resolution modeling framework with a network of in situ measurements of CH_4 and C_2H_6. Luther et al. (2022) used a network of portable solar-tracking Fourier transform spectrometers (EM27/SUN) along with a Lagrangian particle dispersion model to calculate emissions from coal mining activity in Poland. The EM27/SUN is an instrument commonly used to measure column-averaged dry air mole fractions of CH_4 with high precision. Klappenbach et al. (2015) and Knapp et al. (2021) have deployed the portable instrument on ships to measure transects of CH_4 concentrations across the Atlantic and the Pacific Ocean and Hase et al. (2015) have set up EM27/SUN spectrometers in Berlin to determine emissions of CH_4 and CO_2.

In 2019, Dietrich et al. (2021) installed the Munich Urban Carbon Column network (MUCCnet), an urban sensor network, that constantly measures greenhouse gases with EM27/SUN instruments in a fully automated and long-term manner. The network consists of four spectrometers around the city and one at the center such that at least one station will always be upwind and another one downwind. The network of solar-tracking spectrometers measures the total column concentration of CH_4 and thus is sensitive to both near ground and above ground sources.

For this study we temporarily moved part of the MUCCnet infrastructure to Hamburg, and operated four of the spectrometers in locations distributed around the city.

With the third biggest port in Europe (one of the 20 largest in the world (Hafen Hamburg, 2021), Hamburg contains a large industrial area south of the Elbe river, with oil and gas refineries and it is one of the largest cities in Europe. According to the TNO GHGco inventory 3% of total CH_4 emissions in Germany occur in Hamburg (Super et al., 2020). Previous studies in Hamburg targeted only specific parts of the city or specific sources alone. Matousu et al. (2017) estimated the emissions from one part of the river Elbe. Furthermore, Maazallahi et al. (2020) explored gas leakages through mobile measurements in the mostly residential area north of the Elbe.

In this study we aimed at a city scale quantification of CH_4 emissions and thus complement the column measurements, with mobile CH_4 surveys, to get a better understanding of the spatial distribution of sources. Additionally source type attribution was carried out to discriminate between biogenic and thermogenic origin of plumes.

A popular method to explore the types of sources is measuring the isotopic composition of plumes. Menoud et al. (2020), Lu et al. (2021) and Dietrich et al. (2023) use the isotopic signature to reveal the source type. For CH_4, the isotope ratios between ^{13}C and ^{12}C, and between ^{1}H and ^{2}H are particularly meaningful (^{2}H is also denoted with D for Deuterium). Comparing the observed isotope compositions to references from the literature or previous measurements may then indicate the type of sources.

When quantifying CH_4 emissions, usually only one of the concepts of mobile measurements or inversion of column/in-situ measurements is applied. In this study we combined both of them to identify and quantify the sources in a top-down approach. We used a sensor network similar to MUCCnet together with an emission map with updated distributions based on mobile in situ measurements at the street level. The emission estimate is computed based on the updated map and is compared to the estimate based on the original inventory. For instance, Lauvaux et al. (2016) and Jones et al. (2021) already compared different prior emission maps (priors) to improve modeling. Lauvaux et al. (2016) compared two emission maps for CO_2 but both were taken from literature, while our emission maps are updated using mobile measurements, conducted during the
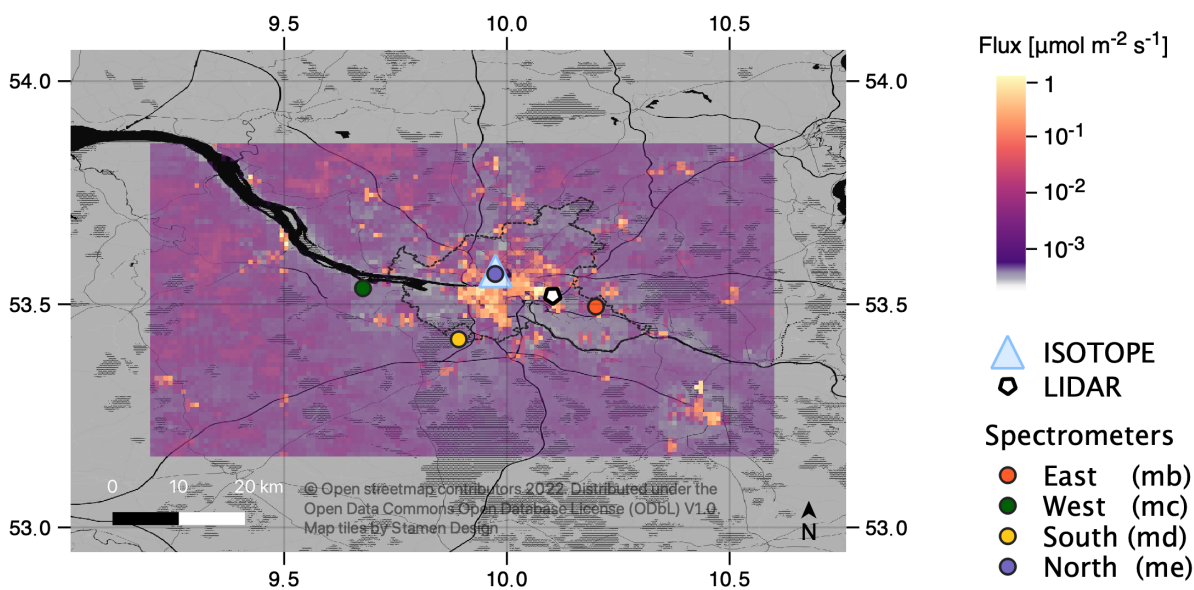
Figure 1. Locations of the FTIR Spectrometers and the wind lidar during the campaign. The original TNO GHGco emission inventory, which was used as a prior estimate for emissions, is shown for the modeling domain. Also the border of the administrative region of Hamburg is shown as a black dashed line. The spectrometer me was co-located with an in-situ CH_4 isotope instrument. The shaded areas indicate forests and wetlands.

campaign. Additionally, we measured the isotopic composition of CH_4 in the city centre of Hamburg continuously for the campaign period, to assign enhancements to biogenic or thermogenic sources. To quantify the uncertainty of the modeled wind field, we deployed a Leosphere Windcube 200S Doppler wind lidar that retrieves vertical profiles of wind direction and speed (Wildmann et al., 2020; Vasiljević et al., 2016).

2 Method

To measure GHG emissions from a large spatial domain and source mix like Hamburg, remote sensing and in-situ measurements were combined. The remote sensing setup consists of four FTIR-Spectrometers, which were deployed around the city as visible in Figure 1. An in-situ CH_4 isotope instrument was co-located with the northern spectrometer and additionally a wind lidar was deployed to measure wind direction and speed.

2.1 FTIR Measurements

Our approach to determine urban emissions is based on the differential column methodology (Chen et al., 2016). The column integrated dry air mole fractions of CO_2, CH_4 and carbon monoxide (CO) are measured with the help of at least two solar-

tracking spectrometers that are placed upwind and downwind of an emission source. The concentration gradients between these stations represent the emissions that are generated in between. The setup in Hamburg consists of four spectrometers to ensure that for most wind directions the differential column condition is met, and a meaningful background can be constrained by the inversion framework. As the wind direction is not constant throughout the measurement period, we placed four spectrometers in different locations around the harbour area where the highest emissions are expected according to the TNO GHGco Inventory (Super et al., 2020). The TNO GHGco Inventory is an European database that includes spatially resolved emission data for CO_2, CH_4, CO, NO_x and NMVOCs. The spatial resolution is $(1/60)°$ for longitude and $(1/120)°$ for latitude, which represents an area of approximately $1.1\,\mathrm{km} \times 0.6\,\mathrm{km}$ in Hamburg. The emissions are divided into 15 gridded nomenclature for reporting (GNFR) sectors. TNO GHGco is currently the highest resolution GHG emission inventory that is available for Hamburg. For this study yearly average emission estimates as recorded in the inventory were considered.

Between the 27th of July 2021 and the 9th of Sept 2021 our four FTIR-Spectrometers were measuring in Hamburg. From 30 July to 5 Sept, the instruments were deployed at the locations shown in Figure 1. Before and after that, side-by-side measurements of the four spectrometers were carried out on a roof at the University of Hamburg to make sure all instruments are properly calibrated to each other (See Figure A2).

The EM27/SUN instruments were deployed in custom enclosures that protect the spectrometer from rainfall and adverse weather conditions (Dietrich et al., 2021; Heinle and Chen, 2018). These enclosures automatically open when the sun is visible, so that sunlight enters the spectrometer. When rainfall is detected, the system shuts its cover so that the spectrometer is protected against precipitation. The instruments are connected to the internet, which enabled us to operate the four spectrometers remotely during a long campaign.

The enclosures were located in the west, the south, the east and in the center of the city of Hamburg as visible in Figure 1. The three sites outside of the city were selected to have little point source influence by local near-by sources and were placed about 20km apart from each other, so the expected CH_4 concentration gradients, predicted by the inventory, between the stations are well above instrument precision. The northern site was co-located with the isotope measurements on top of the roof of the Geomatikum building of the University of Hamburg. This location was chosen weighting different criterions, firstly the availability of sites with suitable conditions to house the room-size setup for isotopic measurements as well as allowing for the set up of the FTIR instruments on top of a flat roof. The second consideration was to place the site outside of the industrial area, a high emission zone according to the TNO GHGco inventory.

The retrieval of concentrations from interferograms was performed using Gfit GGG2014 Wunch et al. (2015) according to Dietrich et al. (2021). The measurements of the column-averaged dry air mole fractions must be properly filtered to exclude measurement errors. In particular, these arise from non-optimal solar tracking, which is mainly caused by clouds. We used two successive filtering steps: The first filtering step is based on physical properties such as solar elevation, absolute solar intensity, and solar intensity variation during a Michelson interferometer scan. The second filtering step uses data statistics to remove outliers and measurement periods with too few data points. In this step measurements are split when for more than 18s no measurement is available. Then each 2 minutes of data are only considered when there is at least continuous measurement data

for more than one minute. This way outliers from partial cloud coverage during the interferometer scan are reduced. Finally, the remaining continuous measurement sections are averaged using a 10 minutes moving average filter. Gaps are not filled.

In order to filter out days with fragmented and interrupted measurements due to repeated cloud cover, we only consider measurement days when at least two stations were measuring at the same time for more than 5 hours. In August 2021 the weather was unexpectedly cloudy and many days the systems were in idle. However, we still had nine good measurement days with sufficient sun-shine to carry out the measurements.

2.2   In-Situ Measurements

To support the modeling and the calculation of the final emission estimate, in situ measurements were performed with a Picarro GasScouter G4302 which measures CH_4 and C_2H_6 and a Picarro G2301 greenhouse gas analyzer which measures CH_4 and CO_2. Both sensors were mounted inside a car and a tube was used to pipe the air from the inlet located on the front bumper into the sensors. The height of the inlet was ca. 60 cm above ground level. The CH_4 concentration measurements with a sampling frequency of 1Hz and 0.3Hz, for the Picarro G4302 and G2301 respectively, were averaged temporally using a moving average with a 10 seconds time window. The averaging improves the precision of the CH_4 measurements from 3 ppb at 1s integration time to 1 ppb at 10 seconds integration time (Chen et al., 2020).

In order to verify and update the prior estimate of an emission map derived from the TNO GHGco Inventory (Super et al., 2020), mobile surveys were conducted in the city and in the industrial area. The first part of the surveys focused on the residential areas of Hamburg mostly to the north of the Elbe and were conducted in the year 2018 by Maazallahi et al. (2020). These were now complemented in 2021 by a mobile survey with the same instruments in the industrial harbour area (All tracks can be seen in Figure 2. The new survey took place between 9th and 21st of August 2021. During the surveys, CH_4, C_2H_6 and CO_2 concentrations were recorded and mapped with a GPS logger. In order to cover the areas in the harbour that were not accessible by public road on the 20th of August, a boat was equipped with the Picarro GasScouter G4302 and additional surveys were carried out on the Elbe river and the waterways in the harbor area. Some private roads in the harbour areas were sampled after permission was granted from the facility owners, including the wastewater treatment plant and two refineries.

The recorded CH_4 concentration during the mobile surveys was separated into its two components, the background and the enhancement peaks occurring near localized sources. While the background is generally rather smooth and varies only slowly with location, the short-time component (peaks in the signal) is caused by emissions of nearby sources. The background signal was determined as the lowest 5th percentile of a ± 2.5 minutes time window around each data point. In order to compile an improved estimate of the spatial distribution of the emissions, both the complete signal (background and enhancement peaks, later referenced as "upd:all") as well as the peaks only (later referenced as "upd:elv") were averaged on the inventory grid, as can be seen in the right and central plot of Figure 3.

The spatial distribution of emissions recorded in the original TNO GHGco inventory was then updated using the mobile concentration measurements. We assumed that in regions where we measured high concentrations, it is more likely to find emission sources than in regions where we measured only background concentrations. The emissions of all inventory pixels

that were covered by our mobile survey were summed up and distributed according to the measured concentrations, weighted according to the number of measurements per pixel.

The following equations show how the original inventory $E(x,y)$ a function of latitude x and longitude y was updated using the concentration measurements $C(x,y)$ averaged on the inventory grid. These measurements were either the whole signal (upd:all) or the peaks only (upd:elev)

First the concentrations were normalized in the area where measurements were available and the emissions recorded in the inventory were re-distributed according to the measured concentrations. The new inventory values N(x,y) were calculated as follows

$$N(x,y) = \frac{C(x,y)}{\sum_{x,y \in C(x,y) \neq NaN} C(x,y)} \sum_{x,y \in C(x,y) \neq NaN} E(x,y). \tag{1}$$

Then a weighting mask $W(x,y)$ was defined according to the number of measurements per pixel.

$$W(x,y) = \frac{count(C(x,y))}{max(count(C(x,y))} \tag{2}$$

New values were mixed between the original inventory value $E(x,y)$ and the new values suggested by Equation 1 according to the weighting mask $W(x,y)$. In pixels with few measurement points, the new emission value of the pixel was chosen closer to the original value of the inventory. In pixels with many measurement points, the value was chosen closer to the value suggested by the concentration-based redistribution of emissions.

$$N_{mixed}(x,y) = E(x,y)(1 - W(x,y)) + W(x,y)N(x,y) \tag{3}$$

The updated inventory $E_{updated}$ is then calculated, depending on the availability of concentration measurements as follows

$$E_{updated}(x,y) = \begin{cases} E(x,y), & x,y \in C(x,y) = NaN \\ \frac{N_{mixed}(x,y)}{\sum_{x,y \in C(x,y) \neq NaN} N_{mixed}(x,y)} \sum_{x,y \in C(x,y) \neq NaN} E(x,y), & x,y \in C(x,y) \neq NaN \end{cases}. \tag{4}$$

For a better comparability between the updated and the original inventory, the sum of emissions in the area covered by our mobile measurements is equal in the original and the updated versions.

The original TNO GHGco inventory has been created using proxy data. For example, all industry emissions reported by Germany were distributed on a map according to the distribution of industrial areas in Germany. In the three inventories used in our study, the industry area south of the Elbe river has lower emissions in the updated versions than in the original inventory, because these emissions were distributed according to the mobile measurements over a wider area.

Furthermore, an inventory layer containing the Elbe and its estimated emissions was added. Matousu et al. (2017) estimated the CH_4 flux from the Elbe into the air for different sections of the river between 0.25 and 4.5 kg h^{-1} km^{-2}. The emission
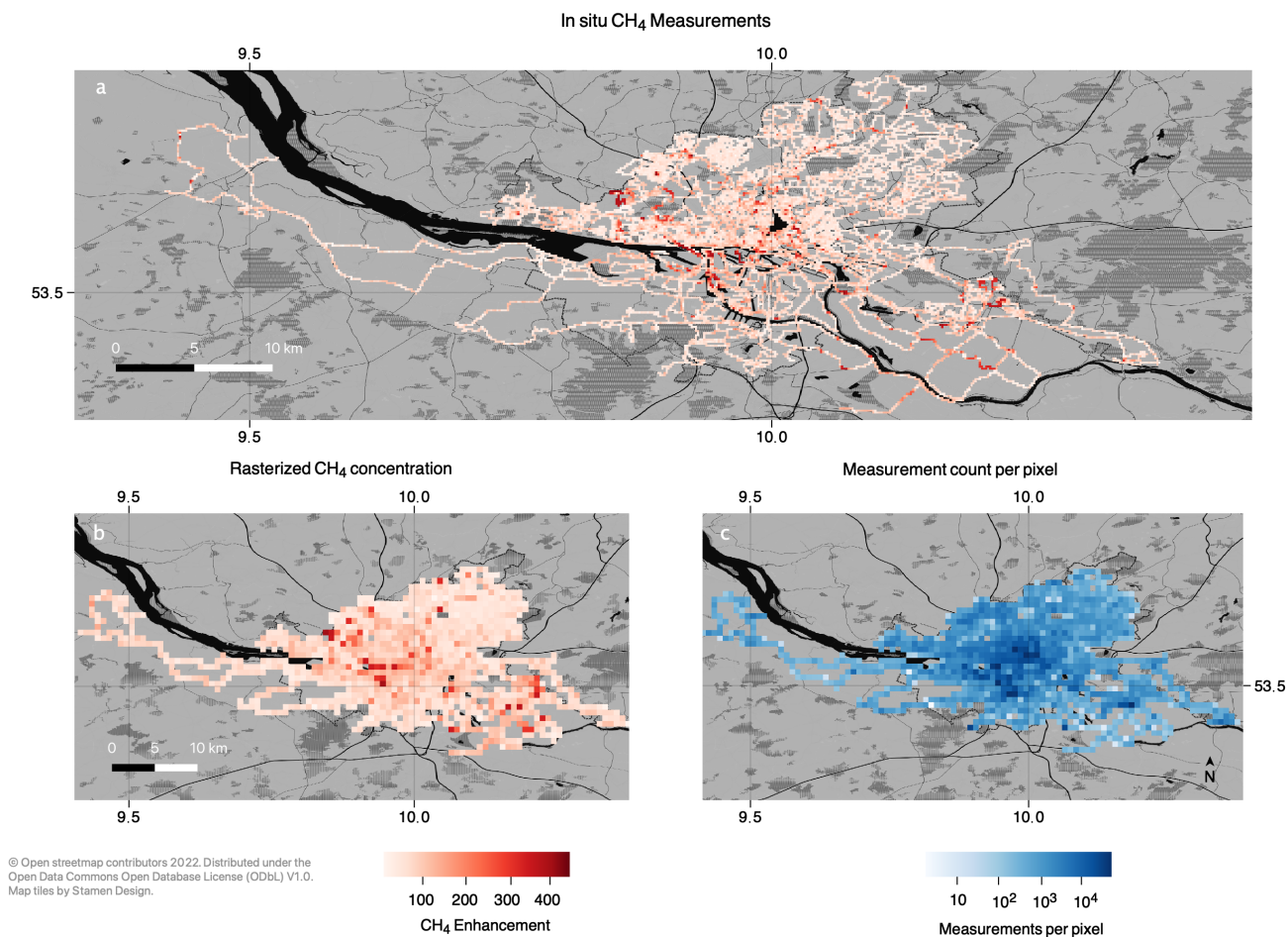
Figure 2. The measured CH$_4$ concentration along the driven tracks recorded during the mobile surveys in 2018 (Maazallahi et al., 2020) and this campaign in 2021 is shown in the left map. The central map shows the concentrations rasterized onto the modeling grid. On the right, the density of measurement points per modeling pixel is plotted.

values for the Elbe in each grid cell is the average flux of the corresponding section multiplied with the proportion of the Elbe inside the grid cell. For parts of the Elbe that were not covered in the study by Matousu et al. (2017), the average emissions of the study (2.5kg h^{-1} km^{-2}) were used as a prior estimate.

During the mobile survey carried out to map concentrations of CH$_4$, multiple transects were driven through observed plumes. Plumes were manually selected when an enhancement higher than 100 ppb was observed. For each plume and location between 3 and 15 transects were driven. Sections, when the car was standing were removed before further analysis. Emission estimates were derived based on a Gaussian plume dispersion model (GPM) as described in Maazallahi et al. (2020). As for several sources the exact emission location was unknown, we calculated an estimate of the emission location for each transect. For this purpose first the possible Pasquille-Gifford stability classes are estimated using wind sensor data, information about the
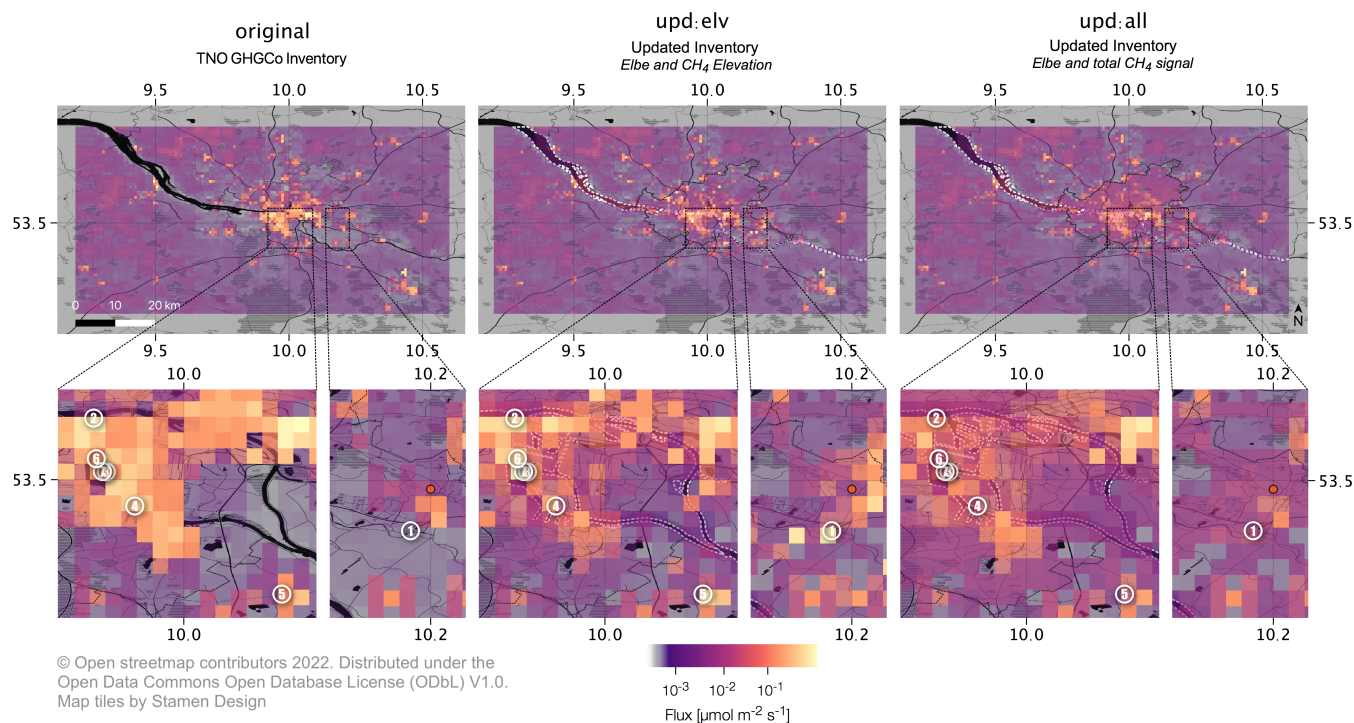
Figure 3. For this study, three different inventories were used. First the original TNO GHGco inventory, secondly the updated inventory using the measured CH_4 enhancement of the mobile survey ("upd:elv"). The third inventory ("upd:all") was updated using the complete CH_4 signal (background+enhancement). All versions of the inventory include an a priori estimate of the river Elbe derived from the findings of Matousu et al. (2017). In this plot, the TNO GHGco Inventory is shown without the Elbe for a better comparison. The close up sections show the locations where point sources were quantified using mobile measurements. Source 3 and 7 are co-located.

daytime and surroundings. In a next step the width of the plume was used to derive σ_y. Under the assumption of a constant stability class, σ_y can be expressed as a function of the distance to the source. This function is independent of the flux and thus an estimate for distance can be determined. The distance in combination with the wind direction lead to an estimate of the location for each transect. For each estimated source location, the flux is then estimated. Errors of the location estimates are propagated into the mean emission estimate. For each location all relevant Pasquill stability classes were estimated. The presented mean emission estimates are the average of estimates obtained for each relevant stability class and location estimate.

2.3 Wind Measurements

During the transect drives, carried out for emissions quantification, wind information close to the ground is important. A local portable wind sensor (Lufft WS200-UMB Smart Weather Sensor), measuring wind direction and wind speed at an altitude of 2m was deployed.

To evaluate the uncertainty of the atmospheric transport of the ERA5 model inside the modeling domain, a Leosphere Windcube 200S Doppler wind lidar was deployed at the Weathermast in Billwerder, Hamburg (See Figure 1). The lidar provides a windprofile from approximately 80m to the top of the atmospheric boundary layer. Measured wind direction and wind speed was compared to the ERA5 model data for all altitudes where model and lidar data was available (See Figure A8). For each measurement day the standard deviation of the differences between ERA5 model and the lidar wind direction and speed was derived.

2.4 Isotope Measurements

On the roof of the Geomatikum building of the University of Hamburg we took continuous measurements of CH_4 at an inlet-height of 80m. Measurements started on the 2nd of August and the setup was operational for most of the campaign period. It was shut down once for maintenance on the 25th of August and resumed operation on the 27th of August. We deployed an Isotope Ratio Mass Spectrometer (IRMS) which continuously measures $\delta^{13}C$ and δD with a Delta V Plus/Deltaplus XL from Thermo Fisher Scientific Inc (Brass and Röckmann, 2010; Röckmann et al., 2016).

In addition to the continuous measurements air samples were taken at several locations while carrying out the mobile survey to characterize the source types of observed plumes similar to Menoud et al. (2021).

To investigate the source mix of the measured CH4 and to decide whether it is mainly of thermogenic or biogenic origin, continuous analysis of the dual stable isotopic composition of CH4 (δ^{13}C and δD) was performed, similar to previous studies (Röckmann et al., 2016; Menoud et al., 2020, 2021). δ^{13}C values are reported versus the Vienna Pee Dee Belemnite (VPDB) standard and δD versus the Vienna Standard Mean Ocean Water (VSMOW).

The dominant source type that is responsible for the observed CH_4 elevations above background in Hamburg was obtained by comparing δD and δ^{13}C values obtained from a Keeling plot analysis (Keeling, 1958) to similar sources signatures in the literature.

Sources were classified as biogenic when δ^{13}C values were between -45 ‰ and -90 ‰ while δD values ranged from -245 ‰ to -360 ‰. Signatures with δ^{13}C values between -32 ‰ and -67 ‰ and a δD value between -118 ‰ and -200 ‰ were attributed to thermogenic emissions (Röckmann et al., 2016).

2.5 Inverse modeling approach

In order to quantify the urban emissions based on the concentration measurements, a Bayesian inversion framework was used. We utilized and adapted the model as presented in Jones et al. (2021) according to the specific requirements of the Hamburg urban area.

This model was designed to quantify diffuse emission sources with the help of several ground-based spectrometers such as the EM27/SUN. The model accounts for temporal variations of the background concentrations using the so called background influence matrix (BIM). Analogous to Jones et al. (2021), supplement S1, virtual particles are released along the line of sight according to the given solar azimuth and elevation angle in 13 altitudes up to 2220m height above the instrument. These particles are released at the receptor time and travel backwards in time until they reach the simulation border (background

time). A weighting factor is assigned to the times when the particles cross the border (background time), based on the number of particles passing the border at that time. It results in a nearly Gaussian shaped distribution of background time for each receptor time. Every $15\,\mathrm{min}$, such a release of particles from each receptor station is initiated. Releasing particles backwards in time is also the basis to generate footprint matrices, which represent the influence of all locations in the domain on the measurement site at a certain receptor time. The footprint is the summation of the residence time of all the particles in a grid cell.

In order to generate those backward trajectories and the footprints, the STILT (Stochastic Time-Inverted Lagrangian Transport) model is used. The meteorological input data for this model is provided by the ERA5 data-set (Muñoz Sabater, 2019).

The TNO GHGco inventory was used as a prior emission map. (Super et al., 2020). Additionally, the updated inventories that are depicted in Figure 3 and described in section 2.2 were compared.

Further assumptions for the model are a spatially homogeneous concentration at the modeling boundary (concentrations can vary with time) and a known spatial distribution of the diffuse emission sources provided by the inventory. The model minimizes a cost function to find for each emission sector the scaling factor that best fits the model to the measurements.

The cost function is described as follows:

$$\mathcal{J}(\mathbf{x}) = \frac{1}{2}(\mathbf{Kx} - \mathbf{y})^{\mathbf{T}}\mathbf{S}_{\varepsilon}^{-1}(\mathbf{Kx} - \mathbf{y}) + \frac{1}{2}(\mathbf{x_a} - \mathbf{x})^{\mathbf{T}}\mathbf{S_a}^{-1}(\mathbf{x_a} - \mathbf{x}) \tag{5}$$

where $\mathbf{x}$ is the unknown that needs to be fitted, which contains the information of the scaling factors for different emission sectors and the background concentration. $\mathbf{K}$ is the sensing matrix that contains the footprints information and BIM. y is the column concentration measurements obtained from the 4 EM27/SUNs. x_a is the prior emission information. S_a and S_ε are the prior error covariance matrices for the prior emission and data-model mismatch.

In this study we use the existing framework developed by Jones et al. (2021) to estimate the emissions for individual days. The total emission estimate for the campaign period was calculated as the weighted average of the individual day results. The average was weighted by the number of measurement points per day. Negative emissions were considered when forming the average.

Emission estimates for smaller areas such as the city of Hamburg or the northern part of Hamburg were calculated by summing up the prior emissions from inventory pixels in that region. This sum was then multiplied with the inversion result for all days of the respective inventory.

2.6 Uncertainty assessment for inverse model

The error assessment follows the approach described in Jones et al. (2021). The uncertainties are extracted from the posterior covariance matrix $\mathbf{S_p}$, which is mathematically computed based on the sensing matrix $\mathbf{K}$ and the prior error covariance matrices $\mathbf{S}_\varepsilon$ and $\mathbf{S_a}$:

$$\mathbf{S_p} = (\mathbf{K^T S}_\varepsilon{}^{-1}\mathbf{K} + \mathbf{S_a}^{-1})^{-1} \tag{6}$$

The uncertainty of the observations ($\sigma^{prior}_{observation}$) was chosen as the sum of instrument precision, which is 0.2 ppb when the measurements are integrated over 10 min (Chen et al., 2016), and the transport error calculated for each day. The transport

error was obtained by simulating a set of footprints for different wind directions. The wind directions were drawn from a normal distribution, with a standard deviation derived for each day by comparing the wind direction of lidar and ERA5 model. No variations were made for the windspeed, as the mean mismatch between lidar and model was as low as 0.49m/s. The resulting set of footprints was then multiplied with the three inventories used in this study to obtain a distribution of prior expected enhancements for all possible wind directions. The standard deviation of this distribution was used as the transport error. $\sigma_{observation}^{prior}$ values are the diagonal elements of $\mathbf{S}_\varepsilon$.

The uncertainty of the prior emission map (σ_{sector}^{prior}) was chosen separately for the river layer and the layer with all anthropogenic sources. The river was given an uncertainty of $\pm 200\%$ and the anthropogenic sector was given an uncertainty of $\pm 100\%$. The uncertainty was chosen higher for the river because a priori information was only available for a section of the river in Matousu et al. (2017) and other areas were estimated with a mean flux of 2.5 kg h^{-1} km $^{-2}$. The uncertainty of the background ($\sigma_{background}^{prior}$) was chosen as 8 ppb according to a comparison of MUCCNet measurements with the Copernicus Atmosphere Monitoring Service (CAMS) data, slightly below the value of 10 ppb used by Jones et al. (2021). σ_{sector}^{prior} and $\sigma_{background}^{prior}$ are the diagonal elements of $\mathbf{S_a}$ as in Jones et al. (2021).

3 Results

3.1 Wind measurements

Wind direction and wind speed model mismatch was calculated for the selected measurement days by comparing lidar data and ERA5 model data. Table 1 shows that in general the windspeed is matched well by the model. A mean difference between model and lidar of 0.49 m/s was recorded (Or in other words, the lidar on average recorded a slightly faster windspeed). The wind direction is off by an average of 6.0 degree.

The calculated mismatch was considered when calculating the transport error for each day as recorded in Table A2. These daily transport error values were then considered in the inversion framework.

During the campaign period there was a good agreement of modeled and measured planetary boundary height as can be seen in Figure A3.

A comparison of wind data from the local sensor (at 2m altitude) used for the GPM emission estimates and the Weathermast (at 10m altitude) showed a mean difference of 1.6m/s (standard deviation of the difference was 1.2m/s) for the wind speed and a mean difference of 15ºCW (standard deviation 31 ºCW) for the wind direction.

3.2 Column Measurements

In Figure 4 the measured concentrations as well as the modeled signal and background is shown for each day. The corresponding emission estimates are shown in Figure 5 for the original inventory and the two updated inventory versions.

On two days, the 23rd of August and the 3rd of September, little enhancement <2 ppb between the stations was observed for most of the time, while the stations were measuring simultaneously. This is visible in Figure 4 by looking at the measurements

Table 1. Comparison ERA5 vs. lidar wind data

Date	Wind speed model mismatch (m/s)		Wind direction model mismatch (ºCW)	
	Mean	Std. Dev.	Mean	Std. Dev.
06 Aug 2021	1.1	1.1	-2.5	24
11 Aug 2021	-0.06	0.91	12	20
12 Aug 2021	-0.07	0.58	-4.8	20
23 Aug 2021	0.70	0.66	6.0	6.5
24 Aug 2021	0.13	0.53	13	11
31 Aug 2021	0.05	0.70	15	10
01 Sep 2021	1.1	0.52	-2.5	13
03 Sep 2021	1.2	0.51	6.3	8.1
05 Sep 2021	0.30	0.57	13	13
mean	0.49	0.7	6.0	16

Standard deviation and mean of the mismatch of wind direction and wind speed between the ERA5 model and lidar data on the selected measurement days. To compute these values the model values have been subtracted from the lidar values.

of the different spectrometers plotted as coloured dots. Small enhancements result in low emission estimates for these days as can be seen by comparing Figure 4 and 5.

On other days, in general, larger enhancements between the stations were observed resulting in larger emission estimates. The 6th, the 11th, the 12th and the 24th of August all show emission estimates higher or equal to the prior. The 1st and the 5th of September have been estimated at values between the prior and zero emissions.

Looking at the result of the 12th of August in Figure 4, it becomes evident that the spectrometer $\mathbf{North}(\mathbf{mc})$ measured a peak at around 12:00 to 13:00 UTC, this peak was not measured by the other stations. During the time of the peak the wind did not change direction and was constantly blowing from the south. Thus the prominent elevation indicates the presence of an unknown temporary source. The inversion framework assigns this elevation to an enhancement of the background concentration (dashed black line at around 10:15 UTC) to balance out observations and prior expected contributions.

On the 31st of August the Spectrometer $\mathbf{West}(\mathbf{mc})$ which was located about 1.5km south from the Elbe river measured an enhancement of about 5 ppb compared to the other stations throughout the whole day, as can be seen in Figure 6 a). During the course of this day the wind came from the north as can be seen by looking at the footprints visualized in white and blue on top of the TNO GHGco Inventory in Figure 6 b).

With the original inventory, the inversion cannot model the enhancement seen by station $\mathbf{West}(\mathbf{mc})$ because there is no large source in the inventory north of the Spectrometer. In such a case the modeled signal, visualized by solid lines in panel a) in Figure 6 do not match the actual measurements (dots) very well. The difference is visible for instance by looking at the distance the blue line (station $\mathbf{West}(\mathbf{mc})$) has from the purple dots in Figure 6.
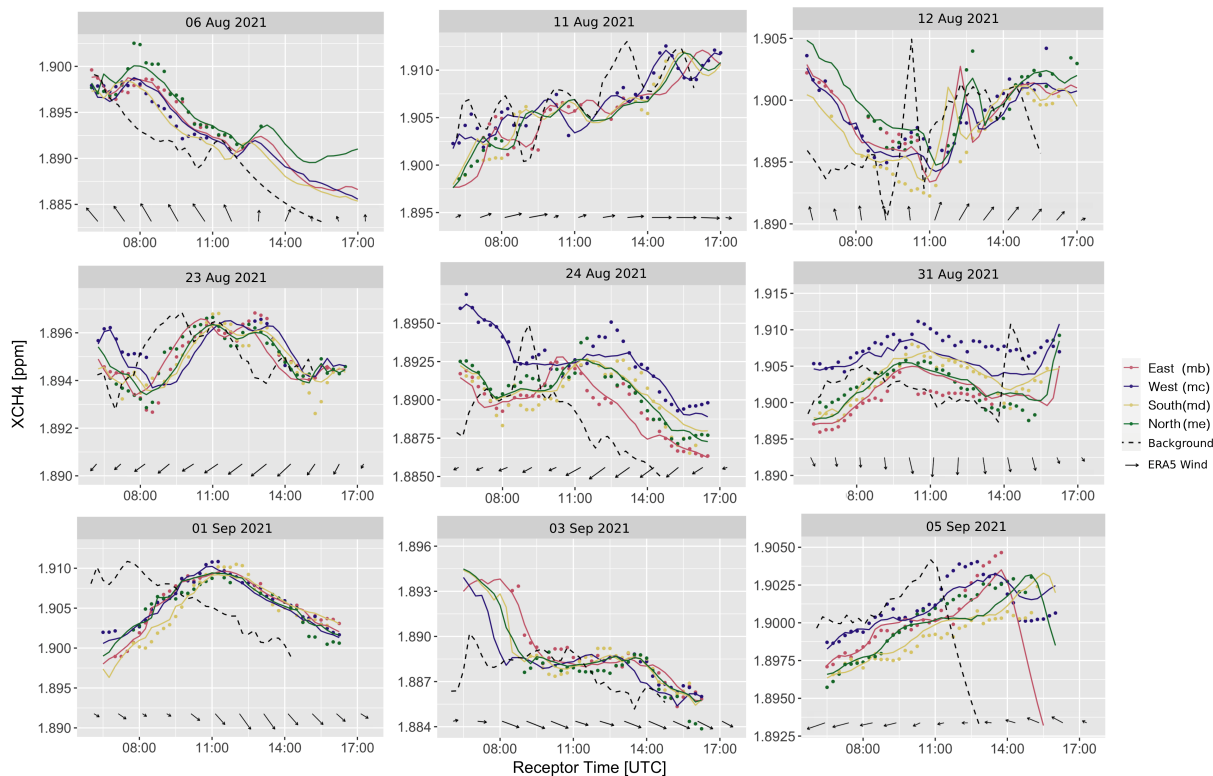
Figure 4. Plot of all selected measurement days as used in the inversion framework. The measurements are plotted as differently colored dots for each station. The colored lines represent the posterior observations generated by the inversion framework and the dashed line shows the fitted background at the domain boundary. Wind direction and relative speed shown as arrows (downward pointing arrows indicate northern wind).

In such a case the modeled background at the domain boundary (black dashed line) gets fitted higher than the signal (solid lines). This can result in negative emission numbers (Figure 6 c)), because the enhancement (measurements - background) becomes negative for most time steps.

When the Elbe river is included in the emission inventory as quantified by Matousu et al. (2017), the modeled signal fits the measurements better and the inversion result returns positive emissions. On this particular day the emissions of the Elbe were quantified much higher than the apriori annual emissions of the Elbe in our domain (350 kg h^{-1}). For consistency we thus decided to include the Elbe river in all other model runs and days presented in this paper. On other days the emissions from the Elbe were close to the prior estimate or around zero as can be seen in Figure A6.

The expected contributions from different sectors for the day 31st of August are shown in Figure 7. These expected contributions were calculated using the footprint and the inventory. As can be seen, on the 31st of August the station **West(mc)** was sensitive to river emissions. Also on the 23rd and 24th of August, as well as on the 5th of September station **West(mc)** was
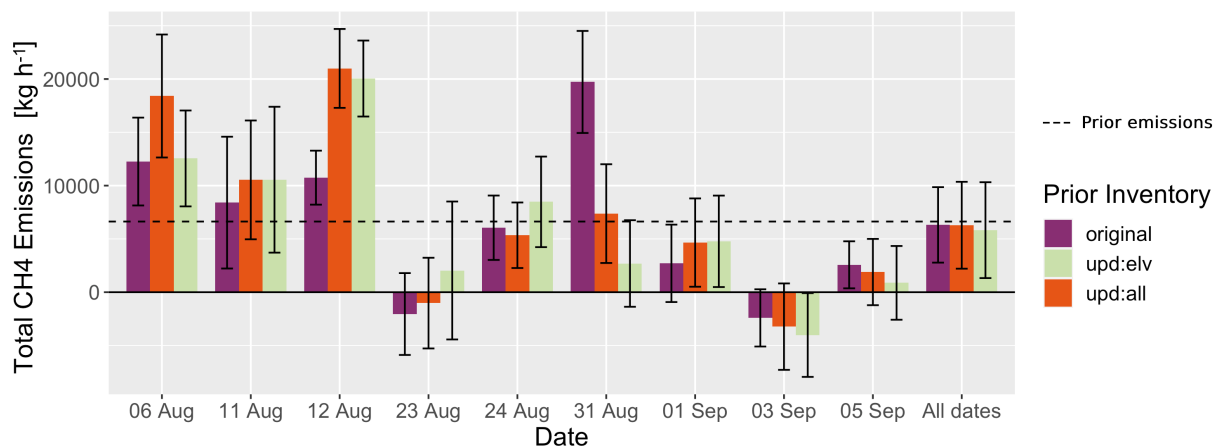
14

Figure 5. Inversion result for all selected days and the three different prior emission inventories ("original": unaltered TNO GHGco inventory, "upd:elv" and "upd:all" are the inventories updated using mobile measurements, filtered for only the peaks as well as the complete measurement signal respectively). The dashed line represents the prior yearly emission estimate of TNO GHGco inventory for the modeling domain. All daily emissions are multiplied up to yearly estimates for better comparison. The emission of the river Elbe was added to all versions of the emission inventory. See Figure A6 in Appendix for the split of total emissions into natural and anthropogenic emissions.

sensitive to river emissions. On all of these days the concentrations measured by station $\mathbf{West(mc)}$ were in general higher than measured by other stations (Compare Figure 4).

3.3 Correlation assessment

For the selected days the correlation between modeled and measured CH_4 concentrations was very high for the total signal (modeled background + enhancement) as can be seen in Figure 8 a). Figure 8 b) shows the correlation for the enhancement only. Modeled enhancements were divided into 0.5 ppb bins and sample means of the first bin (0-0.5 ppb) and the all other bins are significantly distinct (p=0.001) demonstrating quantification of small and large enhancements in total column CH_4 Jones et al. (2021).

The correlation increased significantly when including the natural source into the modeling as visible in Figure A4 in Appendix.

3.4 Comparison of different inventories

In this study three different versions of the emission inventory have been used as a prior estimate for the spatial distribution of CH_4 emissions in Hamburg.

While all three versions lead to comparable results for all measurement days combined, the results differ significantly on single days as can be seen in Figure 5. Over the course of all 9 days the footprint has covered almost all the areas of the
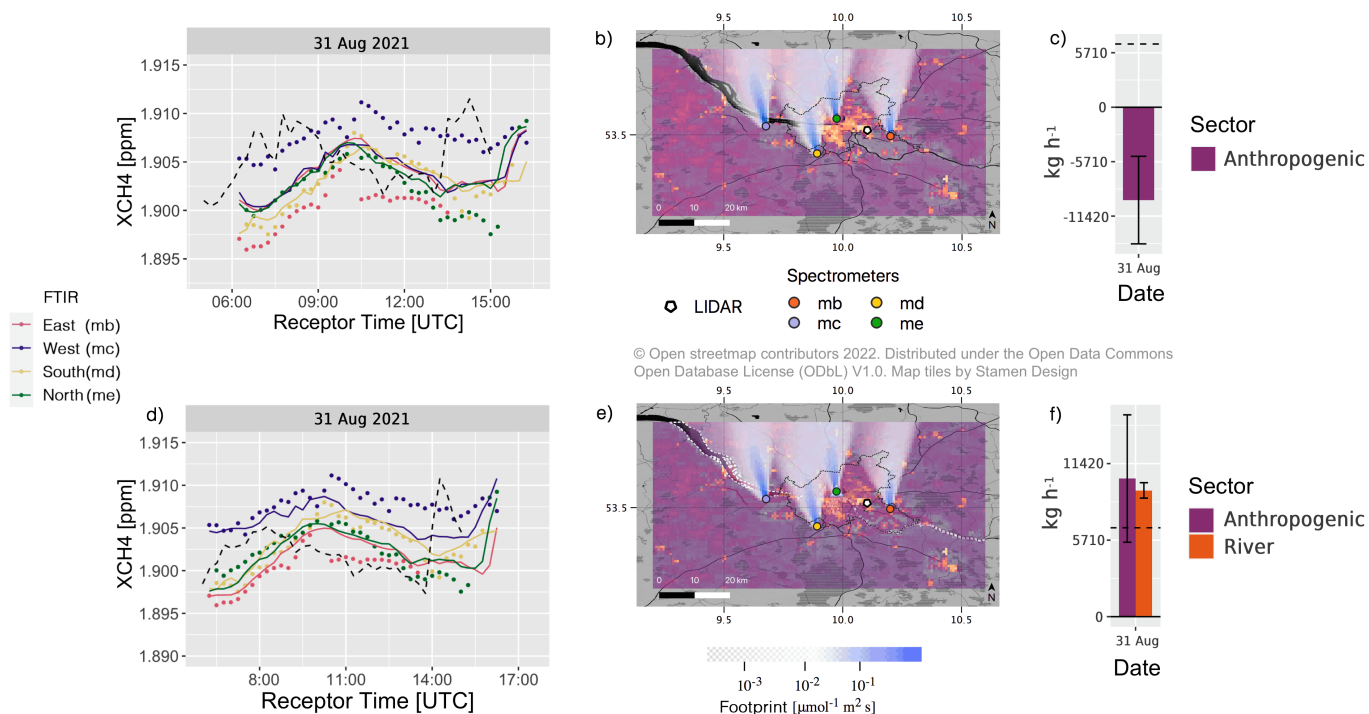
Figure 6. Comparison of the inversion result for different priors on the 31st of August. In the top row the inversion result for the original inventory is shown. The second row shows that the inversion result changes from negative emissions (panel c) to positive emissions (panel f) when the Elbe river is added into the emission inventory (compare the river region, outlined with a dashed white line, in panel b and e). When the river is included in the inventory, the modeled signal (solid line) in panel d) is closer to the measurements (dots) for station **West (mc)** than in panel a. The dashed black line shows the fitted background at the domain boundary.
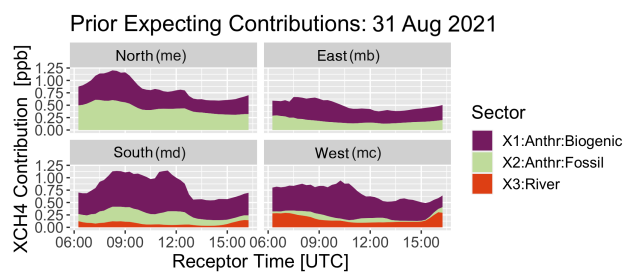
Figure 7. Expected prior contributions from different sectors on the 31st of August for the different stations. **Me** is the northern station, **mb** the eastern station, **md** the southern station and **mc** the western station. Emission estimates are multiplied up to yearly estimates for better comparison.
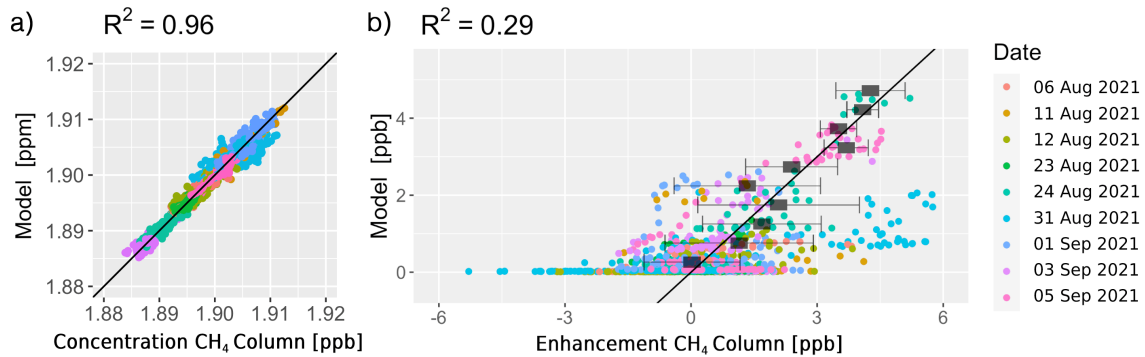
Figure 8. Regression plot of the measured and modeled CH$_4$ signal for all nine selected measurement days. The left plot refers to the whole signal (background and enhancement) while the right plot shows the correlation for the enhancement only. In black a 1:1 line is shown. The black rectangles represent the mean values of the modeled enhancement divided into 0.5 ppb bins. The horizontal error bars represent the sample standard deviation in each bin. The mean of the 0-0.5 ppb bin is significantly different (p=0.001) of the mean of all other bins, which shows that small and large enhancements in total column CH$_4$ can be detected and quantified.

modeling domain (because of different wind directions throughout the campaign), while on single days only small parts of the domain are covered.

355   The difference in emission estimates for the three inventory versions on single days, can be explained by the different spatial distributions of prior emissions. In the area covered by the footprint on a particular day, the recorded emissions can be different in the original and the updated inventories. These differences in prior emissions for each inventory version lead to different scaling factors with the same observations. The scaling factor is determined by the inversion when scaling the three inventory versions to match the forward model and the observations. As all emission inventories are normalized and have the same total 360 emissions a different scaling factor, applied to the whole inventory, can then lead to different total emission estimates.

    For instance, the inversion result can differ with original and the modified inventories, when there is footprint covering the industrial zone of the inventory. This zone has higher emissions in the original inventory than in the two updated versions as visible in the lower left panel of each inventory in Figure 3. With the same observations, the scaling factor calculated by the inversion framework will be slightly lower with the original inventory (as the inventory has already higher emissions recorded 365 here), and higher with the updated inventories, as the updated inventories have lower emissions recorded here.

    For all days the area covered by footprints is covering the domain more uniformly and thus a result in a similar magnitude can be expected for all inventory versions.

3.5   Emission rate estimates from column measurements and comparison to car-based study

We ran the inversion for all inventories (the "original", the "upd:all" and "upd:elv") with the Elbe river as a separate sector. 370 Therefore the emissions are split between river emissions (natural) and anthropogenic sources. We determined the emissions

for the entire modeling domain as well as for the area inside the municipality border of Hamburg. The extent of the modeling domain and the area considered as the city (see Figure 1).

The emission rate estimates for natural and anthropogenic sources combined in our modeling domain sum up to 6300 $\pm$3500 kg h^{-1} for the original inventory, 6300 $\pm$4100 kg h^{-1} for the updated inventory using peaks and background ("upd:all") and 5800 $\pm$4500 kg h^{-1} for the updated inventory using peaks only ("upd:elv") (see Table 2). 1900 $\pm$700 kg h^{-1} of these emissions were attributed to a natural source spanning the whole modeling domain (potentially the Elbe river and associated wetlands).

For the municipal area of Hamburg (including the river, the port, industry and residential zones) natural and anthropogenic CH$_4$ emissions estimated by this study are ranging from 1500 $\pm$1200 kg h^{-1} to 1600 $\pm$920 kg h^{-1}. The CH$_4$ emissions from natural processes for the Hamburg area were estimated as 730 $\pm$270 kg h^{-1} and thus the emissions from anthropogenic sources around 900 $\pm$510 kg h^{-1} (for the original prior).

When we split anthropogenic emissions into biogenic emissions and emissions of thermogenic origin according to the split in the TNO GHGco inventory (see A1), in Hamburg 480 $\pm$260 kg h^{-1} are attributed to thermogenic sources and 420 $\pm$240 kg h^{-1} to man-made biogenic origin, for instance wastewater and landfills (See Figure 10).

If we only look at the part of Hamburg which is located north of the Elbe, which was also studied by Maazallahi et al. (2020) our emission estimate is 420 $\pm$230 kg h^{-1} for anthropogenic sources. This is higher than the 46 $\pm$8.0 kg h^{-1} Maazallahi et al. (2020) report in their study based on up-scaling emissions from a mobile CH$_4$ survey with a car. The difference can be at least partly explained by the different scientific objectives (and thus methodologies) used in both studies. While our study targeted total emission quantification (i.e. from all sources) using column instruments and thus can also capture sources, which are emitting above street level, the in-situ measurements, carried out by Maazallahi et al. (2020) were used to specifically target ground-level emissions near public roads including the identification and and quantification of fugitive emissions from gas pipeline leaks and the sewer system (not including the wastewater treatment plant). If we consider only fugitive emissions according to the TNO split (A1), our study estimates 210 $\pm$110 kg h^{-1} for the northern part of Hamburg. This is between two to eight times higher than the estimate presented by Maazallahi et al. (2020). One potential source which is usually not measurable on the street-level, and could thus explain the lower emissions measured by Maazallahi et al. (2020), is end use inside homes (cook stoves, boilers for heating, etc.) (Lebel et al., 2022; Defratyka et al., 2021). Accumulated emissions from end use, while not affecting street-level concentrations, could be observable in total-column measurements and thus contribute to the higher emission estimates of this study. Another source in Hamburg which could potentially contribute to higher column measurement based estimates is the Alster lake near the city centre. Around this lake Maazallahi et al. (2020) have detected CH$_4$ enhancements, which were low in magnitude but spread over a large area. These low enhancements could not be used for quantification and are thus not included in their estimate, but might be noticeable in the column measurements.

3.6 Emission estimates from mobile survey

For several locations inside the study area emission estimates were derived using a GPM from transects recorded during the mobile survey. All transects for each location were driven on the same day. These estimates are presented in Table 3 and are compared to the emissions recorded in the TNO GHGco inventory as well as the two updated versions. While the emissions

18

Table 2. Emission estimates for modeling domain

	Original	Upd:all	Upd:elv	Inventory
Domain	6300 ±3500	6300 ±4100	5800 ±4500	6600
Natural (Domain)	1900 ±700	1800 ±680	1800 ±700	350
City	1600 ±920	1600 ±1000	1500 ±1200	1500
Anthropogenic (City)	900 ±510	860 ±560	800 ±620	1400
Natural (City)	730 ±270	710 ±270	710 ±280	140

The emission estimates are reported in kg h^{-1} for the different sections of the study area.
"Domain" refers to the entire modeling domain including natural and anthropogenic sources.
"City" refers to natural and anthropogenic emissions calculated for the area inside the municipal
area of Hamburg. "Natural (Dommain)" and "Natural (City)" refer to the emissions from a
natural source in the whole modeling domain and the in the city respectively. Anthropogenic
(City) refers to emissions from anthropogenic activity in the city area.

405 of the two updated inventory versions were only spatially re-distributed according to the recorded spatial distribution of CH$_4$ concentrations, the GPM emission estimates take into account wind information to obtain emission estimates.

For Location 1, an oil refinery, sample bags were analysed and an isotopic signature of thermogenic CH$_4$ emissions was detected. These emissions were quantified as 7.9±5.3 kg h^{-1} by driving multiple transects around the source location as visualized in Figure A5. This value is significantly larger than the value (0.61 kg h^{-1}) recorded in the TNO GHGco inventory

410 for thermogenic CH$_4$ emissions in the corresponding pixel. Also there is no source recorded in the European Pollutant Release and Transfer Register (E-PRTR) (European Environment Agency, 2022), which suggests that it is an unknown source. The updated version of the inventory "upd:all" with a value of 6.4 kg h^{-1} is closest to the Gaussian plume emission estimate for the corresponding inventory pixel. The updated inventory version "upd:elv" suggests even higher emissions for that pixel (76 kg h^{-1}). The fact that the source at Location 1 was observed on several measurement days and was already observed during

415 the measurements in 2018, suggests that this source could have been emitting continuously for a longer time.

At Location 2 north of the Elbe, the industrial area and north of the municipal waste water plant, transects were driven and an emission estimate was derived from the measured plumes as shown in Figure 9. This estimate of 6.7±13 kg h^{-1} has a high relative uncertainty because the estimated source location was far away from the transect lines. The GPM estimate is not significantly different from the values of the original and the two updated inventory versions (5.4 kg h^{-1}, 15 kg h^{-1} and 19

420 kg h^{-1}, respectively). Emissions for this location were estimated during a period of south wind and thus they could originate from various sources from within the industrial area as well as the wastewater treatment plant. At this location no samples were taken because plumes were not always stable.

Location 3 is situated in the industrial complex south of the Elbe near harbour water ways and adjoining several ports used to load or tank boats with gas and oil derived products (See Figure 9). For this location several large plumes were observed on the

425 site of a refinery. These were attributed to thermogenic and biogenic source signatures. Biogenic sources however turned out to be dominant in a Keeling analysis of the sample bags. Biogenic emissions could originate from the near by waterbody or from

fermentation of waste water from the facility. The estimated emissions from this location are 3.1 ± 2.3 kg h^{-1} which confirms the value recorded in the corresponding TNO GHGco Inventory pixel (4.0 kg h^{-1}). The updated inventory version "upd:all" (4.6 kg h^{-1}) is not significantly different from the GPM estimate, while the value in the "upd:elv" version lies significantly higher (40 kg h^{-1}).

The transects at Location 4 were driven on the private roads of a refinery after permission was granted from the operator. First drives were carried out distributed around the accessible area of the refinery and were narrowed down to locations where plumes were detected. The emissions of a prominent point source, present during the time of the survey, were quantified at 1.1 ± 0.7 kg h^{-1} which confirms the values recorded in the TNO GHGco inventory and the updated versions as can be seen in Table 3.

At Location 5 plumes were detected downwind of two large sheds of a farm near Meckelfeld. Isotope measurements of air samples collected at this location indicated a biogenic origin of the source. For this source the "upd:elv" inventory provides the closest estimate of 3.8 kg h^{-1}. The GPM estimate of 8.4 ± 2.5 kg h^{-1} is considerably higher than the values recorded in the original and the "upd:all" version of the inventory (0.55 and 0.87 kg h^{-1}, respectively).

Transects at Locations 6 and 7 were both driven by boat. Two point sources with a magnitude of 6.6 ± 13 kg h^{-1} and 4.5 ± 4.4 kg h^{-1}, respectively, were found in the industrial area. No sample bags were analysed for these locations. For both locations the original inventory is closest to the emission estimate, however the difference between updated and original inventories is small. Both estimates have a high relative uncertainty, because only very few transects were available and the source location could possibly be estimated too far from the transects. Both GPM estimates are not significantly different from the values recorded in the original and updated inventory versions.

In general several significant CH$_4$ sources were quantified during the mobile survey. While several GPM estimates confirmed the values recorded in the emission inventory (both updated and original versions), some of the biogenic and thermogenic sources estimated using GPM, like Location 1 and 5, were significantly above the values recorded in the TNO GHGco inventory. The correlation between GPM estimates and the inventory values is highest for the Upd:elv inventory, $R^2 = 0.13$ compared to $R^2 = 0.10$ and $R^2 = 0.10$ for the Upd:all and the original inventory, respectively. On the other hand side, the Root Mean Square Error (RMSE) is highest for the Upd:elv inventory, 27 kg h^{-1} compared to the Upd:all and the original inventory with a RMSE of 4.4 and 4.1 kg h^{-1}, respectively.

3.7 Comparison with other emission inventories

The emissions from anthropogenic activity in the city of Hamburg were estimated at 900 ± 510 kg h^{-1} which is not significantly different from the 1400 kg h^{-1} reported in the TNO GHGco inventory for the year 2015.

During our study, we observed influence from a biogenic source, which was modeled as river emissions. Large natural area sources such as waterbodies were previously not recorded in the TNO GHGco inventory.

The column-measurement-based CH$_4$ emission estimates for all sectors (natural and anthropogenic sources) in the whole domain, covering the city of Hamburg and parts of the surrounding land outside of Hamburg, are of the same magnitude as reported by inventories, as can be seen in Figure 10.

Table 3. Emission estimates from mobile measurements

L	Lat	Lon	Type	GPM [kg h^{-1}]	Original [kg h^{-1}]	Upd:all [kg h^{-1}]	Upd:elv. [kg h^{-1}]	Signature	Transects	Distance [m]
1	53.468	10.187	refinery	7.9±5.3	0.61	6.4	76	t	12	130±17
2	53.539	9.943	undefined	6.7±13	5.4	15	19	-	6	720 ±240
3	53.505	9.951	refinery	3.1±2.3	4.0	4.6	40.	b	14	220 ±55
4	53.483	9.969	refinery	1.1±0.7	1.5	1.3	1.8	t	11	180 ±40
5	53.427	10.062	farm	8.4±2.5	0.87	0.55	3.8	b	6	310 ±59
6	53.513	9.944	refinery	6.6±13	4.5	2.8	4.1	-	5	220 ±190
7	53.505	9.948	refinery	4.5±4.4	4.9	3.0	4.4	-	4	470 ±200

The emission estimates (GPM) from the mobile survey are reported in kg h^{-1} for selected point sources (L) in the study domain in column "Emission". Estimates are compared to the emissions recorded in the TNO GHGco inventory in column "Original" (without natural emissions). The columns "upd:all" and "Elev." refer to the updated versions of the inventory (including natural emissions). The column "Signature" records the isotopic source signature type t:thermogenic and b:biogenic. Records marked with - were not analysed for source types.

3.8 Isotope measurements

The stationary in-situ measurements on the roof of the Geomatikum building (University of Hamburg) show numerous concentration peaks of around 1 to 2 ppm enhancement, as visible in Figure 11 and A1. During the campaign these peaks were only measured during the night or when the column instrument was not measuring due to cloud cover. Both δ^{13}C and δD Keeling plots yield source signatures which indicate a biogenic origin ($\delta^{13}C$ -61.5 ‰±0.3 ‰, δD =-320 ‰±2.5 ‰) of these peaks, as can be seen in Figure12. Potential sources that have a similar signature are in general microbial sources (Menoud et al., 2021). Both agricultural sources, for instance cattle (Lu et al., 2021) and waste have overlapping signatures with the unknown source in Hamburg. Dietrich et al. (2023) et al. found a similar signature ($\delta^{13}C$ -66.1 ‰, δD =-310 ‰) for air in a subway station. A study on a river estuary at the border between Belgium and the Netherlands by Jacques et al. (2021) found a comparable signature for δ^{13}C (between -25.2 ‰ and -65.6 ‰), however a more enriched signature for δD (between +101 ‰ and -212 ‰). δD signatures of down to -260 ‰ have been measured by Martens et al. (1999) for gassy sediments in an estuary in Germany. The slightly more depleted δD signature measured in this study suggests that the unknown source in Hamburg could be a mix of several different biogenic (microbial) sources. One of these could be a large natural CH$_4$ source, like for instance the river or wetlands that emit in Hamburg (See also section 3.2). The river flow in the city area is however also influenced by anthropogenic activity (harbor traffic, wastewater, etc.) which could contribute to lower δD values. The sharp short-term peaks could be caused by canals in the city close to the in-situ instrument, that fall dry during low tide and then fill up again during high tide.

This hypothesis is supported by the temporal correlation of CH$_4$ peaks with the rising tide as visible in Figure 11. Also less pronounced peaks like in the early morning on the 20th, the 31st of August and the 2nd of September follow this pattern.
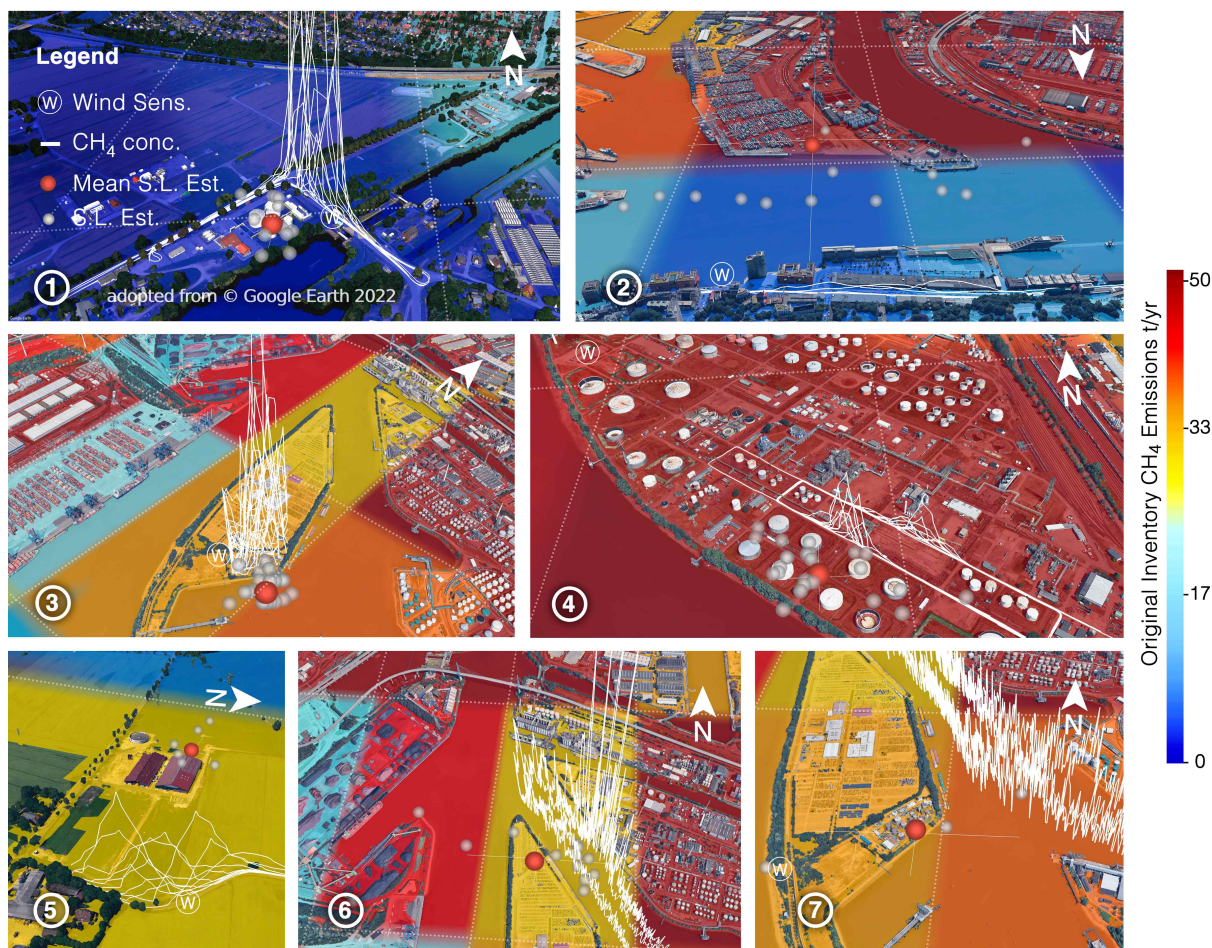
Point sources: GPM quantification

Figure 9. Transects of CH$_4$ concentration measurements are visualized as white lines. These were used to determine the emission strength of point sources with a Gaussian Plume model (GPM). Estimated Source Locations (S.L. Est.) are shown as grey bubbles. The mean source location estimate (Mean S.L. Est.) is shown as a red bubble, with white perpendicular lines indicating the error of the Mean S.L. Est. The background colors indicate the emissions recorded in the original TNO GHGco inventory (biogenic and thermogenic). Inventory pixels are separated by a white dotted line and at this latitude have an approximate length of 1100m and a width of of 650m. Blue areas indicate zones where the original inventory has low emissions recorded, red and yellow areas indicate high emission zones. The locations where a local wind sensor has been mounted, are marked with a "W". Location 6 used the same wind sensor as Location 7. Images taken from Google Earth.

4   Discussion

In our study two ways of correcting the spatial distribution of the prior emission map were attempted. Firstly, the addition of sources quantified by other studies, that are not yet part of standard inventories, such as the TNO GHGco inventory (river
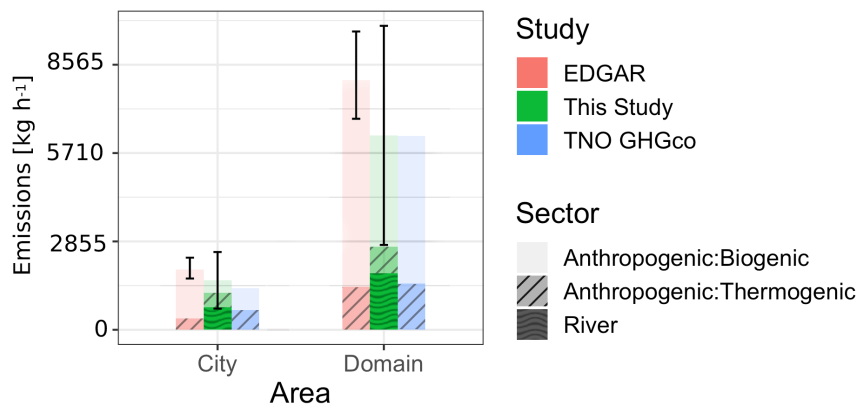
Figure 10. Comparison of Inventories and yearly emission estimates of this study for the city of Hamburg and the whole modeling domain. Emission estimates are split by emission sectors according to the split in the TNO GHGco inventory. Error bars for EDGAR are the overall uncertainties for EDGAR GHG from Solazzo et al. (2021). For the TNO GHGco inventory no uncertainty for CH_4 is available. The TNO GHGco and the EDGAR inventory both do not include river emissions.

emissions were previously reported by Matousu et al. (2017)) and secondly the correction of the spatial distribution of existing gridded inventories via mobile measurements.

485   The example of the 31st of August illustrates how the first approach can have a significant impact on the modeling. When a localized source is not in the inventory, but observable in the measurements, the framework cannot model the prior expected concentrations correctly and thus the modeled enhancement is inexplicably low. In this case the inversion framework will adjust the background to higher values than the measurements and thus can lead to negative enhancements as well as negative emissions. Only when the spatial distribution of the emission sources in the model is representative of the real distribution, the

490   inversion framework is able to constrain the total emissions based on the measurements. Once the river was added as a new source to the emission map, the results turned from negative emissions to positive emissions, which shows that adding unlisted sources to the inventory can improve the modeling significantly. Alternative reasons for the observed behaviour could also be a too low prior uncertainty or sources outside of the domain.

The results for the 31st of August suggest higher emissions from a source north of the western station **mc**. In this paper the

495   source was modeled as river emissions, but it could also be caused by another source further north of the Elbe or outside of the modeling domain. For instance, if there were large cattle farms to the north of **mc**, these could possibly produce similar enhancements and would also match the isotopic signature measured in this study. During the campaign however no mobile survey was conducted in the north of **mc** and the river, which could have revealed emissions from the agricultural sector. Also exceptional emissions from ships circulating on the river could cause or contribute to similar enhancements. Other studies in

500   urban environments, such as a study by Pickard et al. (2021) found that polluted urban lakes in India contribute significantly to CH_4 and CO_2 emissions. Also a study by Zazzeri et al. (2017), who measured isotopic CH_4 signatures in London, suggest that river emissions can contribute significantly to the CH_4 mix. The proximity to the shelf areas of the North sea and the Elbe
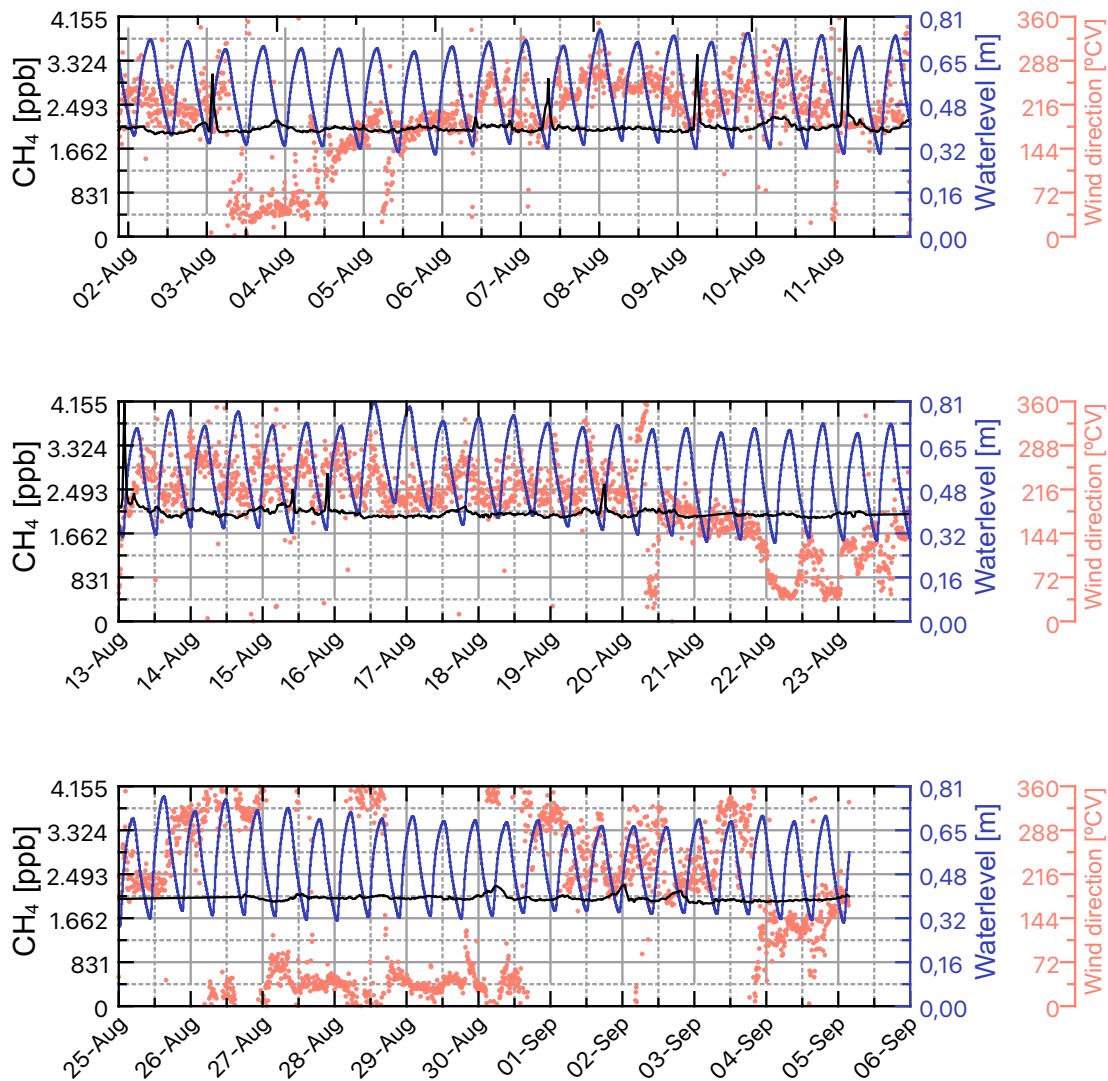
23

Figure 11. In-situ CH$_4$ and wind direction time-series on top of the roof of the Geomatikum, Hamburg. A correlation of the measured peaks with the tide cycle is visible. Water level data from Bundesanstalt für Gewässerkunde (BfG) (2021).

estuary could additionally influence the measurements, as around 75% of ocean CH$_4$ emissions come from these areas (Bange et al., 1994). For natural sources like a river, an oscillation of emissions with the tide cycle could be expected. Such oscillations could however not be resolved in our daily emission estimates derived from column measurements. The analysis of the isotope

505
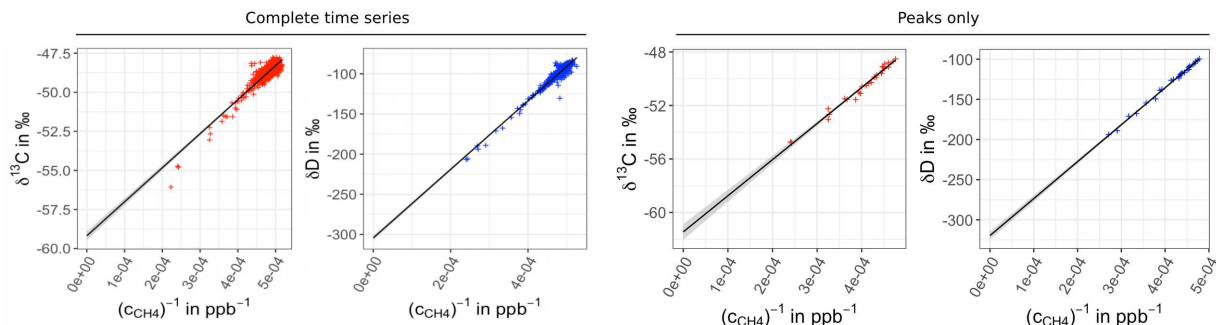
Figure 12. Keeling plot for C and H isotopes once for the complete time series and once for all the CH_4 peaks during the campaign period. Peaks only signature: $\delta^{13}C$ -61.5 ‰±0.3 ‰, δD =-320 ‰±2.5 ‰, Whole time series signature: $\delta^{13}C$ = -58.9 ±0.2 ‰, δD = 306 ±1.5 ‰

in-situ data on the contrary showed such a correlation with the rising tide, which suggests that the peaks could be caused by the river and its connected water bodies.

The inversion framework should in the future be developed further to include in-situ CH_4 emission data along with column concentrations. This way the modeling could be improved and the inversion could further constrain the emission estimates as well as give more insights if the river emissions could in fact explain the observed enhancements.

Other potential sources include CH_4 emissions from soft soil layers, as reported by the city administration for the Elbe glacial valley, which is located mainly to the south of the current river course (Ragnhild Hummel, 2021)). While rather unlikely during a day with moderate wind speeds, these emissions from the ground could have accumulated near the instrument location and caused the observed rise in concentration.

Probably the isotopic signals observed in Hamburg are a mix of several microbial sources of natural and anthropogenic origin. Further investigations here are necessary and mobile measurements near the wetland, which was covered by footprints on the 31st could give a better insight.

Also the second approach, the correction of the spatial distribution of sources with mobile measurements, has an effect, especially on individual days. This may be due to temporal variability of the emissions (different sources emit only for a short period of time) and sometimes the updated inventory matches better, while on other days the original inventory can be used to model the observed enhancements better. In addition to that, on different days, due to specific wind directions, different sections of the inventory are covered with footprints. In some sections the differences between the original and the updated inventories are more pronounced than in other regions. Also it is possible that one of the principal assumptions of the framework, that the background concentration on the whole domain boundary is equal at each time stamp, does not always hold.

The average emission estimate "all Dates" however remains relatively constant for the three versions of the emission inventory. This indicates, that when averaging over multiple measurement days the result is representative for total city emissions and variations in the spatial distribution of prior emissions are of minor importance, whereas they can be important for single

days due to the reasons mentioned above. The variability between individual days is quite large, which could also indicate the limits of the Bayesian inversion for short measurement periods.

530   The correction of the inventory using mobile measurements seems to be a promising approach to update the spatial distribution of emissions. However mobile measurements cannot be carried out everywhere at once and multiple drives over the course of weeks need to be combined to get corrections on a city scale. How representative this relatively short snapshot of measured concentration is of the yearly emissions, needs to be studied further. Nevertheless it should provide a better estimate than bottom up inventories in some cases and could be used to distribute emissions on higher resolution grids in areas where
535   there are no high resolution inventories available.

The combination of the two correction methods, the inclusion of natural sources together with using mobile measurements, can improve the spatial distribution of the prior emission map. Scaling this updated map according to the findings of an inversion framework (using column concentration measurements), turns out to be a feasible technique to update city scale emission inventories. To yield representative emission inventories this approach would need to be carried out for a longer time
540   period, than in the present study, though.

In this study, we have updated all sectors of the emission inventory at once. Since mobile measurements are however only sensitive to near ground sources such as fugitives from gas infrastructure and waste water, in future studies the information obtained from mobile surveys could be used to correct only the corresponding sectors in the inventory.

In order to improve the inversion framework further work is necessary especially regarding approaches on how to find a
545   more reliable background prior. At the moment, a constant value has been used which is then fitted by the framework to the measurements. This can lead to errors especially when the spatial and temporal variations of the emissions in the inventory do not conform to the measured enhancements.

The emission estimate for the city of Hamburg was derived over the period of one and a half months and the GPM estimates were derived during an even shorter time and according to Brantley et al. (2014) might not be representative of yearly emissions.
550   Long term measurements especially in the different seasons of the year are necessary to quantify the quite variable ensemble of sources. Also the prior emission inventory is based on average yearly emissions (summer and winter months), thus the prior emissions could not be fully representative of the study period in the summer.

Natural sources such as the river might be emitting more in the summer, while natural gas fired heating is mainly used in the winter months. The gap between the emission estimate of the mobile survey by Maazallahi et al. (2020) and the column-based
555   estimate derived in this study could, in the future, be investigated further. For instance, measuring indoor fugitive emissions in representative households and up-scaling these results to a city scale could give further insights where the difference is coming from.

During the mobile surveys we visited several refineries in the harbour area. One large refinery was in the process of disassembly, because the industrial site is moving to another location in Germany. This example shows that although the measured
560   emissions being currently lower than the emission inventory suggests, sources such as industrial processing sites might have just moved their facilities and are now emitting somewhere else. Further studies and updated emission inventories are necessary, which take into account the spatial changes of emission sources over time and across administrative borders and countries.

5 Conclusions

This study shows the challenges of quantifying CH_4 emissions of a large source region like the municipal area of Hamburg. The approach using FTIR Spectromenters and a Bayesian inversion framework turned out to be dependent on a correct modeling of the emission sources in the prior emission inventory. The addition of river emissions, which were quantified in a previous study by Matousu et al. (2017), was necessary to obtain positive emission estimates on the 31st of August. Small sources and sectors, could not be quantified separately using this methodology, because the expected concentrations were below the instrument precision. The emission estimate derived in this study has a large uncertainty and estimates from the bottom-up inventories TNO GHGco and EDGAR are not significantly different. Further good measurement days distributed around a year would be needed to get a more certain estimate. Also further improvements to the small-domain inversion system could be made to exclude the possibility of the boundary conditions affecting the emission estimates. Our study shows, that it is feasible to correct the spatial distribution and the magnitude of sources in emission inventories using a combination of mobile measurements and the inversion of column measurements. The addition of natural sources, that are not listed in the inventory, improved the modeling significantly on some days. While the corrections using mobile measurements, changed the emission estimates for particular days, this effect averaged out for the whole campaign period and the "all Dates" estimate was similar for updated and non updated inventories. On the one hand side our analysis of column measurements suggests that there is a large natural CH_4 source, potentially the Elbe river, in Hamburg, which is not listed in common emission inventories. Some standard inventories such as the TNO GHGco inventory do not include natural sources, such as wetlands and rivers and adding these manually to the inventory can improve the modeling. On the other hand side our isotope measurements revealed CH_4 signals which were attributed to a biogenic origin. The timing of the measured CH_4 peaks correlates with the rising tide of the river estuary, which makes a connection between the observed peaks and the river system more likely. Further investigations are necessary to show if this source is in fact the Elbe river and wetlands, or if the calculated natural emissions are a summation of several independent biogenic sources (of natural and anthropogenic origin). The isotope measurements in Hamburg were continued until 28 March 2022 and a future study will give more insights about this in the near future.

Although the contributions from natural sources are significant in Hamburg (730 ± 270 kg h^{-1}), the study also shows that the largest share in the total CH_4 emissions in Hamburg are of anthropogenic origin (900 ± 510 kg h^{-1}). A comparison between an earlier study in Hamburg by Maazallahi et al. (2020) and this study showed that the CH_4 emissions derived via street-level mobile measurements could potentially underestimate total emissions, not capturing natural gas related CH_4 emissions from end use in homes (e.g. gas stoves, boilers for heating; (Lebel et al., 2022; Defratyka et al., 2021; Dietrich et al., 2023)). Also large area sources like for instance the Alster lake or the Elbe, could contribute to the differences in emission estimates. In the course of this study a large and so far unknown emission source of thermogenic origin was located at a refinery and quantified at 7.9 ± 5.3 kg h^{-1} using mobile measurements. This finding highlights the need for further surveys of unknown sources in cities and that an increased effort in the reduction of anthropogenic CH_4 emissions in cities is required.
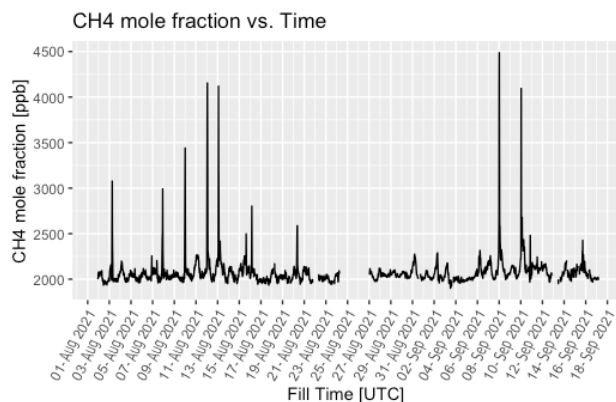
Appendix A

A1 Figures

Figure A1. Stationary in-situ measurements of CH_4 for a longer timeframe. Even after the end of the campaign peaks are visible. These will be discussed in more detail in a future study.
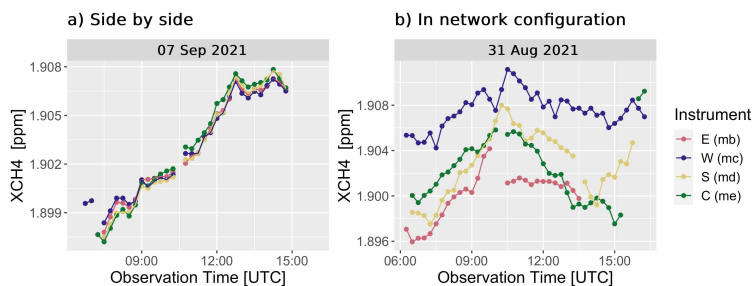

Figure A2. Measurements of the four FTIR instruments after calibration. a) co-located (side by side) on top of the roof of the Geomatikum, Hamburg (mismatch between instruments 0.21 ± 0.48 ppb) and b) in network configuration according to Figure 1.
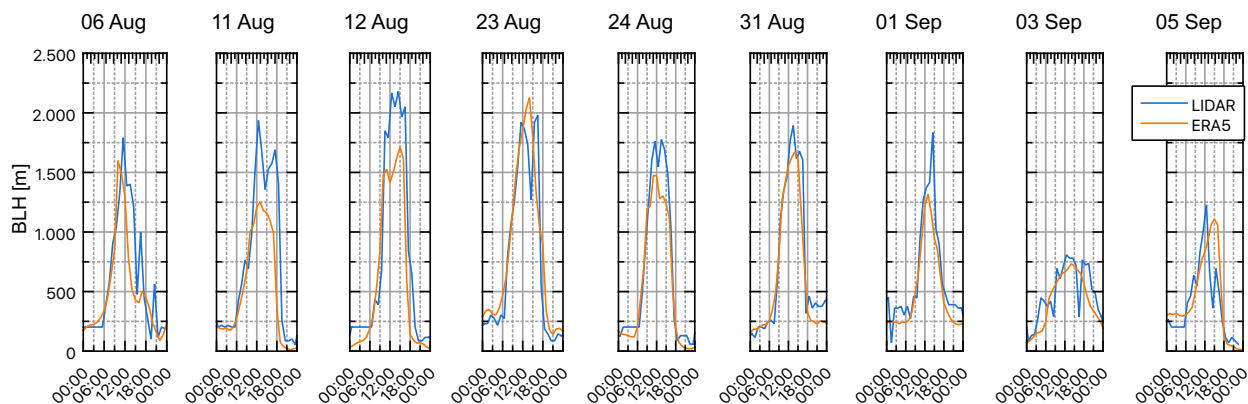
Figure A3. Planetary boundary layer height comparison. Estimate extracted from lidar turbulence measurements versus ERA5 model result. For the campaign period good agreement between model and lidar results was found.
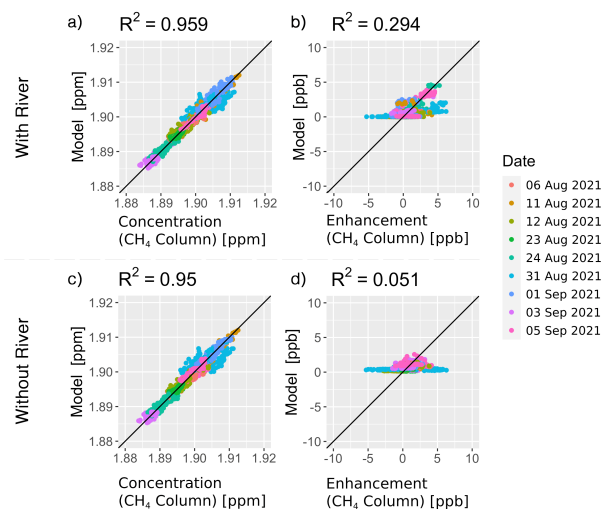
Figure A4. Regression plot of the measured and modelled CH_4 signal for all nine selected measurement days. The top row shows the result for a prior with the river added as a separate sector. The bottom row shows the result using the unchanged TNO GHGco inventory (no river emissions added). The left column refers to the whole signal (background and enhancement) while the right column shows the correlation for the enhancement only. The addition of the river emissions increased the correlation of the enhancement significantly.
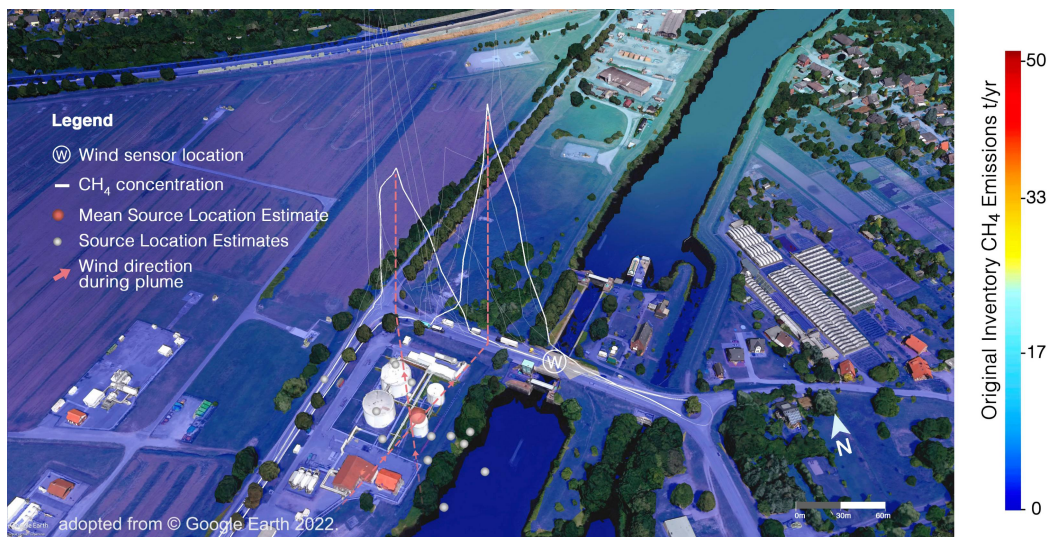
Figure A5. Visualization of the mobile measurements around an oil refinery (Location 1) near Bergedorf, Hamburg. The measured CH_4 plumes are shown as white lines. Two distinct plumes for slightly different wind directions are highlighted. For all recorded plume-transects a source location estimate has been derived (grey balls). The mean estimate for the source location is shown as a red ball co-located with one of the refinery tanks. The background colors indicate the emissions recorded in the original TNO GHGco inventory. Blue areas indicate zones where the original inventory has low emissions recorded.
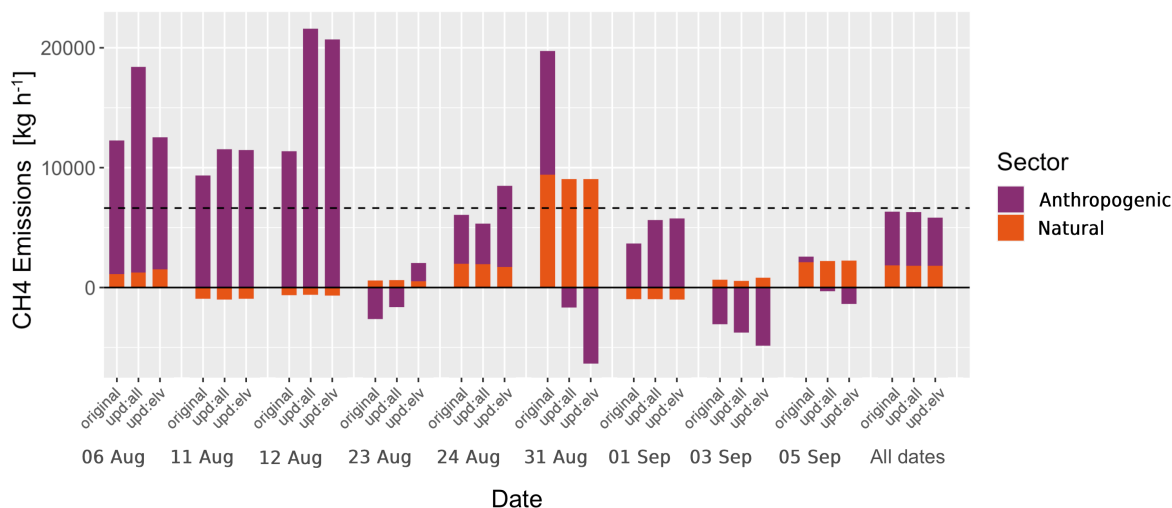
Figure A6. The results of the inversion split by the two sectors (River and anthropogenic) used in the modelling. Emission estimates are multiplied up to yearly estimates.
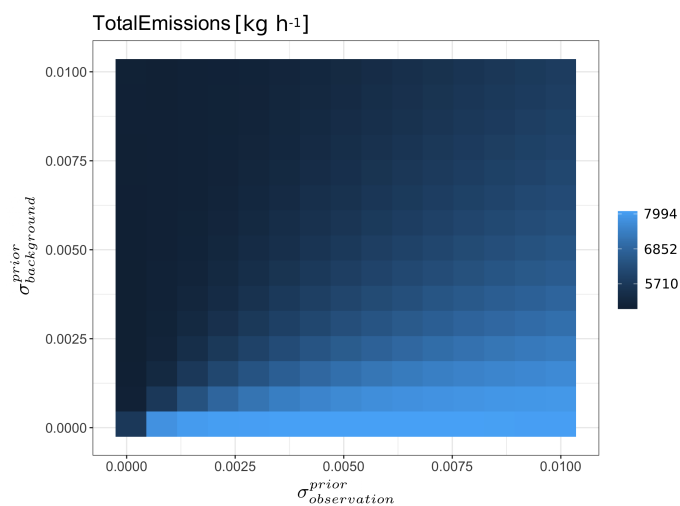
Figure A7. The two inversion parameters $\sigma^{prior}_{observation}$ and $\sigma^{prior}_{background}$, which represent the uncertainties of the observations and the background estimate respectively, have been varied systematically. The final emissions for the whole domain are shown for each parameter combination in this plot. Emissions are quite stable for all realistic parameter combinations.
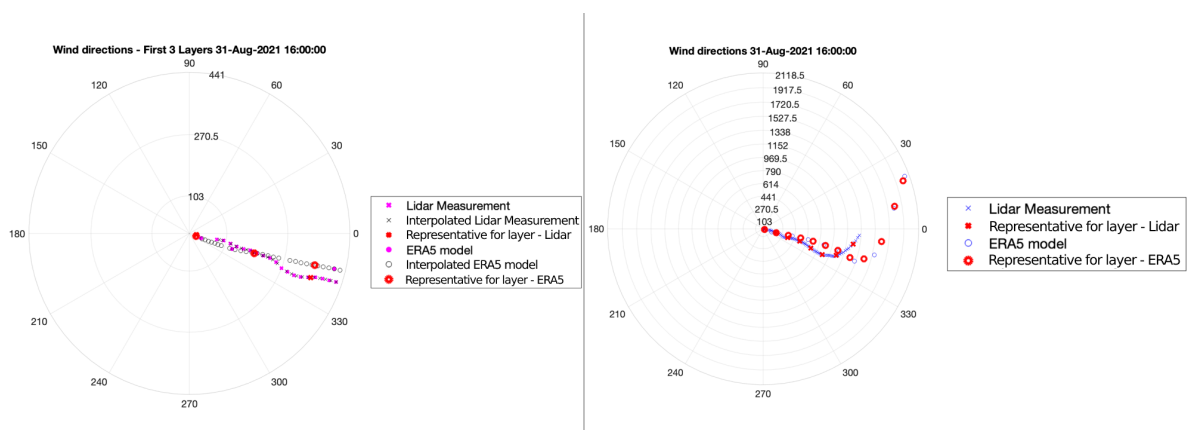
Figure A8. Comparison of LIDAR wind data and ERA5 Model data on the 31st of August. The circles in the wind-rose plot correspond to different altitudes in meter. The wind direction (in degrees) is plotted for each height level. The left figure is a zoomed in version of the right figure and shows how measurement and model results were interpolated for the comparison. In this left figure raw data is represented by the color magenta, interpolated data is represented by the color black, and the representative for each height layer is represented by the color red. The angular distance between the red circles and red crosses in each plot corresponds to the wind direction mismatch in each layer. The right figure shows all the height levels used to compute mismatch.

A2 Tables

Table A1. Assignment of inventory sectors to the categories biogenic and thermogenic

Inventory	Thermogenic		Biogenic	
	Abbreviation	*Description*	*Abbreviation*	*Description*
	CHE	Chemical processes	AGS	Agricultural soils
	ENE	Power industry	AWB	Agricultural waste burning
	FFF	Fossil fuel fires	ENF	Enteric fermentation
	IND	Combustion for manufacturing	MNM	Manure management
	IRO	Iron and steel production	SWD	Solid waste
EDGAR	PRO	Fuel exploitation		
	RCO	Energy for buildings	WWT	Waste water handling
	REF TRF	Oil refineries and Transformation industry		
	TNR	Aviation, shipping, railway		
	TRO	Road transportation		
	A	Public Power	K	Agricultural Livestock
	B	Industry	L	Agricultural Other
	C	Other Stationary Combustion	J	Waste
	D	Fugitives		
TNO	E	Solvents		
	F1-3	Road transportation		
	G	Shipping		
	H	Aviation		
	I	Off-road		

Classification of the different source sectors in the TNO and EDGAR inventory in biogenic and thermogenic emissions. Given that the TNO inventory does not separate waste into sub-categories, we treated all the sources from waste in the EDGAR inventory as one for consistency

Table A2. Transport error in ppm

Date	Upd:Elv	Upd:All	Original
06 Aug 2021	0,00072	0,00062	0,00066
11 Aug 2021	0,00071	0,00068	0,00070
12 Aug 2021	0,00056	0,00053	0,00053
23 Aug 2021	0,00056	0,00053	0,00056
24 Aug 2021	0,00074	0,00068	0,00082
31 Aug 2021	0,00073	0,00074	0,00073
01 Sep 2021	0,00098	0,00101	0,00105
03 Sep 2021	0,00078	0,00066	0,00075
05 Sep 2021	0,00119	0,00101	0,00110

Average transport error in ppm as calculated for each day and each of the three inventories ("Upd:all" and "Upd:elv", as well as the original TNO GHGco inventory), by rotating the trajectories of the particle files according to the standard deviation of the Lidar vs. ERA5 Model miss-match

Table A3. Average ERA5 and lidar wind data

Date	Mean Wind Speed (m/s)		Mean Wind Direction (ºCW)	
	Lidar	Model	Lidar	Model
06 Aug 2021	6,1	5,0	158	160
11 Aug 2021	4,1	4,1	273	261
12 Aug 2021	4,2	4,2	192	197
23 Aug 2021	7,5	6,8	55	49
24 Aug 2021	4,0	3,9	73	60
31 Aug 2021	4,6	4,6	8	354
01 Sep 2021	5,4	4,3	312	314
03 Sep 2021	6,3	5,1	298	291
05 Sep 2021	2,8	2,5	102	89

Daily mean wind direction and wind speed (model and lidar data) for selected campaign days that were used to estimate emissions.

References

Allen, D. T., Torres, V. M., Thomas, J., Sullivan, D. W., Harrison, M., Hendler, A., Herndon, S. C., Kolb, C. E., Fraser, M. P., Hill, A. D., Lamb, B. K., Miskimins, J., Sawyer, R. F., and Seinfeld, J. H.: Measurements of methane emissions at natural gas production sites in the United States, Proceedings of the National Academy of Sciences, 110, 17 768–17 773, https://doi.org/10.1073/pnas.1304880110, publisher: National Academy of Sciences Section: Physical Sciences, 2013.

Bange, H. W., Bartell, U. H., Rapsomanikis, S., and Andreae, M. O.: Methane in the Baltic and North Seas and a reassessment of the marine emissions of methane, Global Biogeochemical Cycles, 8, 465–480, https://doi.org/https://doi.org/10.1029/94GB02181, 1994.

Brantley, H., Thoma, E., Squier, W., Guven, B., and Lyon, D.: Assessment of Methane Emissions from Oil and Gas Production Pads using Mobile Measurements, Environmental science technology, 48, https://doi.org/10.1021/es503070q, 2014.

Brass, M. and Röckmann, T.: Continuous-flow isotope ratio mass spectrometry method for carbon and hydrogen isotope measurements on atmospheric methane, Atmospheric Measurement Techniques, 3, 1707–1721, https://doi.org/10.5194/amt-3-1707-2010, publisher: Copernicus GmbH, 2010.

Bundesanstalt für Gewässerkunde (BfG): Wasserstraßen- und Schifffahrtsverwaltung des Bundes (WSV), https://www.pegelonline.wsv.de/webservices/files/Wasserstand+Rohdaten/ELBE/HAMBURG+ST.+PAULI, 2021.

Chen, J., Viatte, C., Hedelius, J. K., Jones, T., Franklin, J. E., Parker, H., Gottlieb, E. W., Wennberg, P. O., Dubey, M. K., and Wofsy, S. C.: Differential column measurements using compact solar-tracking spectrometers, Atmospheric Chemistry and Physics, 16, 8479–8498, https://doi.org/10.5194/acp-16-8479-2016, publisher: Copernicus GmbH, 2016.

Chen, J., Dietrich, F., Maazallahi, H., Forstmaier, A., Winkler, D., Hofmann, M. E. G., Denier van der Gon, H., and Röckmann, T.: Methane emissions from the Munich Oktoberfest, Atmospheric Chemistry and Physics, 20, 3683–3696, https://doi.org/10.5194/acp-20-3683-2020, publisher: Copernicus GmbH, 2020.

Defratyka, S. M., Paris, J.-D., Yver-Kwok, C., Fernandez, J. M., Korben, P., and Bousquet, P.: Mapping urban methane sources in Paris, France, Environmental Science & Technology, 55, 8583–8591, 2021.

Dietrich, F., Chen, J., Voggenreiter, B., Aigner, P., Nachtigall, N., and Reger, B.: MUCCnet: Munich Urban Carbon Column network, Atmospheric Measurement Techniques, 14, 1111–1126, https://doi.org/10.5194/amt-14-1111-2021, 2021.

Dietrich, F., Chen, J., Shekhar, A., Lober, S., Krämer, K., Leggett, G., van der Veen, C., Velzeboer, I., Denier van der Gon, H., and Röckmann, T.: Climate Impact Comparison of Electric and Gas-Powered End-User Appliances, Earth's Future, 11, e2022EF002 877, https://doi.org/https://doi.org/10.1029/2022EF002877, e2022EF002877 2022EF002877, 2023.

European Environment Agency: European Industry Emissions Portal, https://industry.eea.europa.eu/explore/explore-data-map/map, 2022.

Fernandez, J., Maazallahi, H., France, J., Menoud, M., Corbu, M., Ardelean, M., Calcan, A., Townsend-Small, A., van der Veen, C., Fisher, R., et al.: Street-level methane emissions of Bucharest, Romania and the dominance of urban wastewater., Atmospheric Environment: X, 13, 100 153, 2022.

Hafen Hamburg: Top 20 Containerhäfen, https://www.hafen-hamburg.de/de/statistiken/top-20-containerhaefen/, 2021.

Hase, F., Frey, M., Blumenstock, T., Groß, J., Kiel, M., Kohlhepp, R., Mengistu Tsidu, G., Schäfer, K., Sha, M. K., and Orphal, J.: Application of portable FTIR spectrometers for detecting greenhouse gas emissions of the major city Berlin, Atmospheric Measurement Techniques, 8, 3059–3068, https://doi.org/10.5194/amt-8-3059-2015, publisher: Copernicus GmbH, 2015.

Heinle, L. and Chen, J.: Automated enclosure and protection system for compact solar-tracking spectrometers, Atmospheric Measurement Techniques, 11, 2173–2185, https://doi.org/10.5194/amt-11-2173-2018, 2018.

IPCC, I. et al.: Climate change 2014: Synthesis report. Contribution of working groups I, II and III to the fifth assessment report of the intergovernmental panel on climate change, 2014.

Jacques, C., Gkritzalis, T., Tison, J.-L., Hartley, T., Van der Veen, C., Röckmann, T., Middelburg, J. J., Cattrijsse, A., Egger, M., Dehairs, F., et al.: Carbon and hydrogen isotope signatures of dissolved methane in the Scheldt Estuary, Estuaries and Coasts, 44, 137–146, 2021.

Jones, T. S., Franklin, J. E., Chen, J., Dietrich, F., Hajny, K. D., Paetzold, J. C., Wenzel, A., Gately, C., Gottlieb, E., Parker, H., Dubey, M., Hase, F., Shepson, P. B., Mielke, L. H., and Wofsy, S. C.: Assessing Urban Methane Emissions using Column Observing Portable FTIR Spectrometers and a Novel Bayesian Inversion Framework, Atmospheric Chemistry and Physics Discussions, pp. 1–30, https://doi.org/10.5194/acp-2020-1262, publisher: Copernicus GmbH, 2021.

Keeling, C. D.: The concentration and isotopic abundances of atmospheric carbon dioxide in rural areas, Geochimica et Cosmochimica Acta, 13, 322–334, https://doi.org/10.1016/0016-7037(58)90033-4, 1958.

Klappenbach, F., Bertleff, M., Kostinek, J., Hase, F., Blumenstock, T., Agusti-Panareda, A., Razinger, M., and Butz, A.: Accurate mobile remote sensing of XCO_2 and XCH_4 latitudinal transects from aboard a research vessel, Atmospheric Measurement Techniques, 8, 5023–5038, https://doi.org/10.5194/amt-8-5023-2015, 2015.

Knapp, M., Kleinschek, R., Hase, F., Agustí-Panareda, A., Inness, A., Barré, J., Landgraf, J., Borsdorff, T., Kinne, S., and Butz, A.: Shipborne measurements of XCO_2, XCH_4, and XCO above the Pacific Ocean and comparison to CAMS atmospheric analyses and S5P/TROPOMI, Earth System Science Data, 13, 199–211, https://doi.org/10.5194/essd-13-199-2021, 2021.

Lauvaux, T., Miles, N. L., Deng, A., Richardson, S. J., Cambaliza, M. O., Davis, K. J., Gaudet, B., Gurney, K. R., Huang, J., O'Keefe, D., Song, Y., Karion, A., Oda, T., Patarasuk, R., Razlivanov, I., Sarmiento, D., Shepson, P., Sweeney, C., Turnbull, J., and Wu, K.: High-resolution atmospheric inversion of urban CO2 emissions during the dormant season of the Indianapolis Flux Experiment (INFLUX), Journal of Geophysical Research: Atmospheres, 121, 5213–5236, https://doi.org/10.1002/2015JD024473, _eprint: https://onlinelibrary.wiley.com/doi/pdf/10.1002/2015JD024473, 2016.

Lebel, E. D., Finnegan, C. J., Ouyang, Z., and Jackson, R. B.: Methane and NOx Emissions from Natural Gas Stoves, Cooktops, and Ovens in Residential Homes, Environmental Science & Technology, 56, 2529–2539, https://doi.org/10.1021/acs.est.1c04707, pMID: 35081712, 2022.

Lu, X., Harris, S. J., Fisher, R. E., France, J. L., Nisbet, E. G., Lowry, D., Röckmann, T., van der Veen, C., Menoud, M., Schwietzke, S., and Kelly, B. F. J.: Isotopic signatures of major methane sources in the coal seam gas fields and adjacent agricultural districts, Queensland, Australia, Atmospheric Chemistry and Physics, 21, 10 527–10 555, https://doi.org/10.5194/acp-21-10527-2021, publisher: Copernicus GmbH, 2021.

Luther, A., Kostinek, J., Kleinschek, R., Defratyka, S., Stanisavljević, M., Forstmaier, A., Dandocsi, A., Scheidweiler, L., Dubravica, D., Wildmann, N., Hase, F., Frey, M., Chen, J., Dietrich, F., Necki, J., Swolkień, J., Knote, C., Vardag, S., Roiger, A., and Butz, A.: Observational constraints on methane emissions from Polish coal mines using a ground-based remote sensing network, Atmospheric Chemistry and Physics, 22, https://doi.org/10.5194/acp-22-5859-2022, 2022.

Maazallahi, H., Fernandez, J. M., Menoud, M., Zavala-Araiza, D., Weller, Z. D., Schwietzke, S., von Fischer, J. C., Denier van der Gon, H., and Röckmann, T.: Methane mapping, emission quantification, and attribution in two European cities: Utrecht (NL) and Hamburg (DE), Atmospheric Chemistry and Physics, 20, 14 717–14 740, https://doi.org/10.5194/acp-20-14717-2020, publisher: Copernicus GmbH, 2020.

Martens, C. S., Albert, D. B., and Alperin, M. J.: Stable isotope tracing of anaerobic methane oxidation in the gassy sediments of Eckernfoerde Bay, German Baltic Sea, American Journal of Science, 299, 589–610, https://doi.org/10.2475/ajs.299.7-9.589, 1999.

Matousu, A., Osudar, R., Simek, K., and Bussmann, I.: Methane distribution and methane oxidation in the water column of the Elbe estuary, Germany, Aquatic Sciences, 79, 443–458, 2017.

McKain, K., Down, A., Raciti, S. M., Budney, J., Hutyra, L. R., Floerchinger, C., Herndon, S. C., Nehrkorn, T., Zahniser, M. S., Jackson, R. B., Phillips, N., and Wofsy, S. C.: Methane emissions from natural gas infrastructure and use in the urban region of Boston, Massachusetts, Proceedings of the National Academy of Sciences, 112, 1941–1946, https://doi.org/10.1073/pnas.1416261112, publisher: National Academy of Sciences Section: Physical Sciences, 2015.

Menoud, M., van der Veen, C., Scheeren, B., Chen, H., Szénási, B., Morales, R. P., Pison, I., Bousquet, P., Brunner, D., and Röckmann, T.: Characterisation of methane sources in Lutjewad, The Netherlands, using quasi-continuous isotopic composition measurements, Tellus B: Chemical and Physical Meteorology, 72, 1–20, https://doi.org/10.1080/16000889.2020.1823733, publisher: Taylor & Francis _eprint: https://doi.org/10.1080/16000889.2020.1823733, 2020.

Menoud, M., van der Veen, C., Necki, J., Bartyzel, J., Szénási, B., Stanisavljević, M., Pison, I., Bousquet, P., and Röckmann, T.: Methane (CH_4) sources in Krakow, Poland: insights from isotope analysis, Atmospheric Chemistry and Physics, 21, 13167–13185, https://doi.org/10.5194/acp-21-13167-2021, 2021.

Muñoz Sabater, J.: ERA5-Land hourly data from 1981 to present. Copernicus Climate Change Service (C3S) Climate Data Store (CDS)., https://cds.climate.copernicus.eu/cdsapp/dataset/reanalysis-era5-land?tab=overview ,Accessed on 20.09.2021, 2019.

Phillips, N. G., Ackley, R., Crosson, E. R., Down, A., Hutyra, L. R., Brondfield, M., Karr, J. D., Zhao, K., and Jackson, R. B.: Mapping urban pipeline leaks: Methane leaks across Boston, Environmental Pollution, 173, 1–4, https://doi.org/10.1016/j.envpol.2012.11.003, 2013.

Pickard, A., White, S., Bhattacharyya, S., Carvalho, L., Dobel, A., Drewer, J., Jamwal, P., and Helfter, C.: Greenhouse gas budgets of severely polluted urban lakes in India, Science of The Total Environment, 798, 149019, https://doi.org/10.1016/j.scitotenv.2021.149019, 2021.

Prather, M. J., Holmes, C. D., and Hsu, J.: Reactive greenhouse gas scenarios: Systematic exploration of uncertainties and the role of atmospheric chemistry, Geophysical Research Letters, 39, https://doi.org/10.1029/2012GL051440, _eprint: https://onlinelibrary.wiley.com/doi/pdf/10.1029/2012GL051440, 2012.

Ragnhild Hummel, P. E.: Methan aus Weichschichten - Sicheres Bauen bei Bodenluftbelastung, https://www.hamburg.de/contentblob/2854392/1f4da8e6be01aa72de913be2470593d4/data/d-bodenluftbelastung-broschuere.pdf, 2021.

Röckmann, T., Eyer, S., van der Veen, C., Popa, M. E., Tuzson, B., Monteil, G., Houweling, S., Harris, E., Brunner, D., Fischer, H., Zazzeri, G., Lowry, D., Nisbet, E. G., Brand, W. A., Necki, J. M., Emmenegger, L., and Mohn, J.: In situ observations of the isotopic composition of methane at the Cabauw tall tower site, Atmospheric Chemistry and Physics, 16, 10469–10487, https://doi.org/10.5194/acp-16-10469-2016, 2016.

Sargent, M. R., Floerchinger, C., McKain, K., Budney, J., Gottlieb, E. W., Hutyra, L. R., Rudek, J., and Wofsy, S. C.: Majority of US urban natural gas emissions unaccounted for in inventories, Proceedings of the National Academy of Sciences, 118, https://doi.org/10.1073/pnas.2105804118, 2021.

Schwietzke, S., Griffin, W. M., Matthews, H. S., and Bruhwiler, L. M. P.: Natural Gas Fugitive Emissions Rates Constrained by Global Atmospheric Methane and Ethane, Environmental Science & Technology, 48, 7714–7722, https://doi.org/10.1021/es501204c, publisher: American Chemical Society, 2014.

Solazzo, E., Crippa, M., Guizzardi, D., Muntean, M., Choulga, M., and Janssens-Maenhout, G.: Uncertainties in the Emissions Database for Global Atmospheric Research (EDGAR) emission inventory of greenhouse gases, Atmospheric Chemistry and Physics, 21, 5655–5683, https://doi.org/10.5194/acp-21-5655-2021, publisher: Copernicus GmbH, 2021.

Super, I., Dellaert, S. N. C., Visschedijk, A. J. H., and Denier van der Gon, H. A. C.: Uncertainty analysis of a European high-resolution emission inventory of CO_2 and CO to support inverse modelling and network design, Atmospheric Chemistry and Physics, 20, 1795–1816, https://doi.org/10.5194/acp-20-1795-2020, 2020.

Toja-Silva, F., Chen, J., Hachinger, S., and Hase, F.: CFD simulation of CO2 dispersion from urban thermal power plant: Analysis of turbulent Schmidt number and comparison with Gaussian plume model and measurements, Journal of Wind Engineering and Industrial Aerodynamics, 169, 177–193, https://doi.org/10.1016/j.jweia.2017.07.015, 2017.

Vasiljević, N., Lea, G., Courtney, M., Cariou, J.-P., Mann, J., and Mikkelsen, T.: Long-Range WindScanner System, Remote Sensing, 8, https://doi.org/10.3390/rs8110896, 2016.

von Fischer, J. C., Cooley, D., Chamberlain, S., Gaylord, A., Griebenow, C. J., Hamburg, S. P., Salo, J., Schumacher, R., Theobald, D., and Ham, J.: Rapid, Vehicle-Based Identification of Location and Magnitude of Urban Natural Gas Pipeline Leaks, Environmental Science & Technology, 51, 4091–4099, https://doi.org/10.1021/acs.est.6b06095, publisher: American Chemical Society, 2017.

Weller, Z. D., Roscioli, J. R., Daube, W. C., Lamb, B. K., Ferrara, T. W., Brewer, P. E., and von Fischer, J. C.: Vehicle-Based Methane Surveys for Finding Natural Gas Leaks and Estimating Their Size: Validation and Uncertainty, Environmental Science & Technology, 52, 11 922–11 930, https://doi.org/10.1021/acs.est.8b03135, publisher: American Chemical Society, 2018.

Weller, Z. D., Yang, D. K., and von Fischer, J. C.: An open source algorithm to detect natural gas leaks from mobile methane survey data, PLOS ONE, 14, 1–18, https://doi.org/10.1371/journal.pone.0212287, 2019.

Wildmann, N., Päschke, E., Roiger, A., and Mallaun, C.: Towards improved turbulence estimation with Doppler wind lidar velocity-azimuth display (VAD) scans, Atmospheric Measurement Techniques, 13, 4141–4158, https://doi.org/10.5194/amt-13-4141-2020, 2020.

Wunch, D., Toon, G. C., Sherlock, V., Deutscher, N. M., Liu, C., Feist, D. G., and Wennberg, P. O.: Documentation for the 2014 TCCON Data Release, https://doi.org/10.14291/TCCON.GGG2014.DOCUMENTATION.R0/1221662, 2015.

Yacovitch, T. I., Herndon, S. C., Pétron, G., Kofler, J., Lyon, D., Zahniser, M. S., and Kolb, C. E.: Mobile Laboratory Observations of Methane Emissions in the Barnett Shale Region, Environmental Science & Technology, 49, 7889–7895, https://doi.org/10.1021/es506352j, publisher: American Chemical Society, 2015.

Zazzeri, G., Lowry, D., Fisher, R., France, J., Lanoisellé, M., Grimmond, C. S. B., and Nisbet, E.: Evaluating methane inventories by isotopic analysis in the London region, Scientific reports, 7, 1–13, 2017.